Title

Simple steps to enable reproducibility: culture conditions affecting Chlamydomonas growth and elemental composition

Journal

The Plant Journal, 111(4)

ISSN

0960-7412

Authors

Hui, Colleen
Schmollinger, Stefan
Strenkert, Daniela
et al.

Publication Date

2022-08-01

DOI

10.1111/tpj.15867

Peer reviewed

Simple steps to enable reproducibility: culture conditions affecting Chlamydomonas growth and elemental composition

Colleen Hui[1,2,3], Stefan Schmollinger[1,3], Daniela Strenkert[1,3], Kristen Holbrook[1,#], Hayden R. Montgomery[1], Si Chen[4], Hosea M. Nelson[1,&], Peter K. Weber[5] and Sabeeha S. Merchant[1,3,6,7,§]

Authors institution(s)/affiliation(s)

1 Department of Chemistry and Biochemistry, University of California, Los Angeles CA 90095, USA

2 Chemical Sciences Division, Lawrence Livermore National Laboratory, Livermore, CA 94550, USA

3 California Institute for Quantitative Biosciences (QB3), University of California, Berkeley, CA 94720, USA

4 Advanced Photon Source, Argonne National Laboratory, Argonne, IL 60439, USA

5 Lawrence Livermore National Laboratory, Physical and Life Science Directorate, Livermore, CA 94550, USA

6 Department of Molecular and Cell Biology, University of California, Berkeley, CA 94720, USA

7 Department of Plant and Microbial Biology, University of California, Berkeley, CA 94720, USA

Present address: Amgen Inc, 1 Amgen Center Drive, Thousand Oaks, CA 91320

& Present address: Department of Chemistry, California Institute of Technology, Pasadena, CA 91125, USA

Colleen Hui (https://orcid.org/0000-0002-5543-7440)
Stefan Schmollinger (https://orcid.org/0000-0002-7487-8014)
Daniela Strenkert (https://orcid.org/0000-0002-3420-1332)
Kristen Holbrook (https://orcid.org/0000-0001-6923-3580)
Hayden Montgomery (https://orcid.org/0000-0002-6750-0830)
Si Chen (https://orcid.org/0000-0001-6619-2699)
Hosea M. Nelson (https://orcid.org/0000-0002-4666-2793)

Peter K. Weber (https://orcid.org/0000-0001-6022-6050)
Sabeeha S. Merchant (https://orcid.org/0000-0002-2594-509X)

Running title: Simple steps to not ruin reproducibility

Keywords: ICP, iron, elemental composition, ionome, stress, *Chlamydomonas reinhardtii*

The author responsible for distribution of materials integral to the findings presented in this article is:

Sabeeha S. Merchant
(sabeeha@berkeley.edu)
University of California, Berkeley
408B Stanley Hall
Berkeley, CA 94720-3220

Summary

Even subtle modifications in growth conditions elicit acclimation responses affecting the molecular and elemental makeup of organisms, both in the laboratory and in natural habitats. We systematically explored the effect of temperature, pH, nutrient availability, culture density and access to CO_2 and O_2 in laboratory-grown algal cultures on growth rate, the ionome, and the ability to accumulate Fe. We found algal cells accumulate Fe in alkaline conditions, even more so when excess Fe is present, coinciding with a reduced growth rate. Using a combination of Fe-specific dyes, X-ray fluorescence microscopy and NanoSIMS, we show that the alkaline-accumulated Fe was intracellularly sequestered into acidocalcisomes, which are localized towards the periphery of the cells. At high photon flux densities, Zn and Ca specifically over-accumulate, while Zn alone accumulates at low temperatures. The impact of aeration was probed by reducing shaking speeds and changing vessel fill-levels; the former increased the Cu quota of cultures, the latter resulted in a reduction in P, Ca, and Mn at low fill-levels. Trace element quotas were also affected in stationary phase, where specifically Fe, Cu and Zn accumulate. Cu accumulation here depends inversely on the Fe concentration of the medium. Individual laboratory strains accumulate Ca, P and Cu to different levels. All together, we identified a set of specific changes to growth rate, elemental composition, and the capacity to store Fe in response to subtle differences in culturing conditions of Chlamydomonas, affecting experimental reproducibility. Accordingly, we recommend that these variables be recorded and reported as associated metadata.

Introduction

Even small changes in environmental conditions can result in acclimation responses affecting gene expression, protein composition, enzymatic rates, metabolite pool sizes, and even the elemental makeup of organisms (Demmig-Adams *et al.*, 2008, Salt *et al.*, 2008). For microorganisms, the local temperature, pH, nutrient availability, and culture density are crucial components of their habitats. These aspects are also critical for successful, reproducible cultivation of an organism in laboratory conditions, especially for assessment of quantitative molecular outputs. Photosynthetic microorganisms additionally require adequate gas exchange (especially for CO_2 supply) and light, in terms of both quantity and quality (Bonente *et al.*, 2012, Berger *et al.*, 2014, Erickson *et al.*, 2015). Acclimation to perceived changes in their environment is a common cause for experimental variation in laboratory conditions and a cause of poor reproducibility between different research groups, individual studies, or even individual growth chambers within the same experiment (Massonnet *et al.*, 2010, Porter *et al.*, 2015).

Iron (Fe) is an essential trace element for life because it facilitates a wide range of reactions, most importantly as a cofactor in electron transport and redox chemistry (Crichton, 2008). Fe proteins are involved in DNA synthesis and repair, oxidative stress mitigation, fatty acid metabolism, and respiration. In photosynthetic organisms, the demand for Fe is particularly high, since Fe is additionally used as a cofactor in the abundant complexes of the photosynthetic electron transfer chain (Merchant, 2010, Blaby-Haas and Merchant, 2013, Glaesener *et al.*, 2013). Excess Fe within the cell can lead to the generation of deleterious reactive oxygen species (ROS) through the Fenton reaction (Imlay, 2006, Imlay, 2008) and/or promote mis-metalation, which harms cellular integrity (Imlay, 2014). As a result, the metabolism of Fe is under homeostatic control, which ensures adequate Fe to support metabolism but sequestration of excess (e.g. to ferritin or vacuoles) to prevent undesired reactions (Theil, 1987, Sharma *et al.*, 2016, Schmollinger *et al.*, 2021). The poor solubility of Fe species in aerobic conditions and the pH dependence of Fe solubility means that Fe nutrition is another source of experimental variability.

Factors like temperature, pH, aeration, and other components of the growth medium (*e.g.* carbon, nitrogen sources) can affect Fe bioavailability directly (solubility/oxidation state) and/or cellular metabolism more generally, which in turn affects the intracellular Fe quota,

i.e. the amount of Fe required to satisfy the metabolic demand. For example, changing fluxes in O_2/CO_2 supply may trigger metabolic changes affecting the amount of the abundant Fe-containing proteins in respiratory/photosynthetic complexes, or the amount of Zn-containing carbonic anhydrases, consequently affecting cellular trace metal quotas. The quotas for other micronutrients, including copper (Cu) and manganese (Mn), are likewise dependent on external factors. It is estimated that ~ 40% of all enzymes require trace metal ions as cofactors (Andreini *et al.*, 2008, Waldron *et al.*, 2009). Changes in the expression of abundant enzymes can be reflected in the trace metal quota of the cell (Baxter *et al.*, 2008, Salt *et al.*, 2008). Monitoring the elemental composition or ionome of cells is therefore a quantitative way to assess changes in an organism's enzyme inventory (Baxter *et al.*, 2008).

For over three decades, the eukaryotic unicellular green alga *Chlamydomonas reinhardtii* has been used as a reference organism for the study of trace metal metabolism in photosynthetic organisms (Merchant, 2010, Merchant and Helmann, 2012, Blaby-Haas and Merchant, 2013, Merchant *et al.*, 2020). Chlamydomonas is an important model organism for fundamental research in algae and a crucial reference for biotechnological applications like the production of bio-fuels and -products in algae (Stephenson *et al.*, 2011, Gimpel *et al.*, 2013). Moreover, Chlamydomonas is in the Viridiplantae and shares a common ancestry and many biochemical features with land plants, including the photosynthetic apparatus (Shen *et al.*, 2019, Huang *et al.*, 2021). Chlamydomonas has retained genes and features that were present in the common ancestor to both plants and animals (*e.g.* assembly and motility of eukaryotic cilia/flagella), making it also a useful reference organism outside of the plant kingdom (Silflow and Lefebvre, 2001, Pazour and Witman, 2009). Microorganisms like Chlamydomonas can be grown in a highly controlled manner in the laboratory, utilizing chemically-defined growth media and well-controlled growth incubators. Chlamydomonas is a facultative phototroph that can produce ATP and reducing equivalents either by photosynthesis or by consuming reduced carbon sources, most prominently acetate (Sager and Granick, 1953, Harris, 2008). Chlamydomonas displays extensive metabolic flexibility, adding complexity to its enzyme portfolio, which is documented in its genome size/content (Grossman *et al.*, 2007, Merchant *et al.*, 2007). Because of the advent of 'omics methodologies, which give sensitive readouts of

acclimation responses in well-used reference organisms like Chlamydomonas, it is important to understand the organism's sensitivity and responses to growth parameters. Here, we systematically investigate the influence of changes to temperature, pH, culture density, light intensity and aeration in a physiological range in otherwise strictly controlled culture conditions on the growth and the ionome of Chlamydomonas cells, in particular the trace element quotas and their ability to store Fe.

Results

P, Ca, Fe, Cu and Zn accumulate in stationary phase Chlamydomonas

First, we analyzed growth, elemental composition and Fe over-accumulation (storage) in cultures at different cell densities. Cell density of batch-culture grown photosynthetic microorganisms also impacts access to light, which potentially affects enzyme composition even within the three standard defined growth stages (lag, log, stationary). When culture density increases, light penetration decreases proportionally (Figure 1 A). Cells were collected during the logarithmic growth phase at 1, 2, 4, 6, 8 x 10^6 cells/ml and during stationary phase at 12 and 14 x 10^6 cells/ml and subsequently every 24 h for three additional days. In order to assess Fe storage capacity, we used Fe-replete and Fe-excess media (20 vs. 200 µM Fe, respectively). The elemental content was normalized to total cellular S content, which did not change between the two Fe concentrations or at any point during growth (Supplemental Figure 1). Excess Fe did not alter the growth rate nor the cell density in stationary phase (Figure 1 B-D), which is consistent with previous studies (Moseley *et al.*, 2002, Long and Merchant, 2008). In terms of elemental composition, during logarithmic growth phase, from 1 x 10^6 cells/ml to 8 x 10^6 cells/ml, we did not observe any meaningful changes to the trace metal quotas in the cultures; even between replete and excess Fe conditions, the elemental composition was very similar (Figure 1 E-J). We did, however, observe changes to the trace nutrient contents in stationary cells. Most prominently, Fe, Cu, and Zn increased at stationary phase compared to logarithmic growth conditions, while the total cellular Mn content did not (Figure 1 E-H). Unlike in the logarithmic growth phase, where the trace element quota was comparable at different cell densities, stationary phase cultures showed a linear increase of Fe, Cu, and Zn content over an extended period. While Zn accumulated to a similar extent in both 20 and 200 µM Fe media (Figure 1 G), about twice as much Fe accumulated in the 200 µM Fe medium (Figure 1 E). Cu accumulation showed the opposite effect and accumulated to a higher level in Fe-replete conditions (20 µM, Figure 1 F).

Chlamydomonas was recently shown to utilize the acidic, cytosolic acidocalcisomes as storage organelles for Cu, Mn and Fe (Hong-Hermesdorf *et al.*, 2014, Tsednee *et al.*, 2019, Schmollinger *et al.*, 2021). Acidocalcisomes are rich in Ca and P (Docampo *et al.*,

1995, Scott *et al.*, 1997), which was the motivation for their inclusion in this analysis. Unlike the trace elements, Ca and P accumulation increased immediately after cells reached stationary densities (96 h), but did not increase further over time (Figure 1 I,J).

In order to identify proteins that contribute to the accumulation of different elements in stationary cells, we re-analyzed an RNA sequencing dataset that investigates differential gene expression in logarithmic ($2x10^6$ cells/ml) and late logarithmic ($8x10^6$ cells/ml) (Kropat *et al.*, 2015) or four-days stationary cultures (Lv *et al.*, 2013). We compiled a list of transporters involved in Fe, Cu, Zn, P and Ca uptake, and for reference included an analysis of the transcript abundance changes of these genes in response to Fe, Cu, Zn, P limitation (Moseley *et al.*, 2006, Castruita *et al.*, 2011, Blaby-Haas and Merchant, 2012, Urzica *et al.*, 2012, Malasarn *et al.*, 2013, Schmollinger *et al.*, 2014, Wang *et al.*, 2020, Pivato and Ballottari, 2021). Stationary cells indeed showed increased accumulation of transcripts from two phosphate transporters (PHT) of the PHT4 subfamily, *PHT4D* and *PHT4F* (Supplemental Figure 2). *PHT4D* had previously been found to be induced in P limitation (Schmollinger *et al.*, 2014), while *PHT4F* responds to Fe limitation (Urzica *et al.*, 2012). In late logarithmic cells *CTR2* and two Ca transporters were found to be induced. Many phosphate transporters show high induction upon P starvation, but, interestingly, different subsets of phosphate transporters appear to be induced in response to other stimuli. *PTA3* and *PTA4* are only induced in Cu limitation, not upon P starvation, with *PTA4* also responding to Fe depletion, albeit to a lesser degree. *PTB9* and *PTB12* are induced in Zn limited conditions, but in contrast to the members of the PTA family described above, both genes are also activated in P limitation, and *PTB12* also responds to Fe limitation (Supplemental Figure 2). High affinity transporters involved in Fe, Cu, Zn and Mn acquisition appear to not be induced in stationary cultures (Supplemental Figure 2). The Fe uptake genes were instead induced in Fe-limited cultures as well as in Cu deficiency, where Fe proteins are involved in managing some of the fallout of reduced Cu availability (Merchant and Bogorad, 1986, Moseley *et al.*, 2000). RNA abundances of Fe assimilation proteins in Zn and P limitation were found to be reduced (Supplemental Figure 2). Expression of genes involved in Cu assimilation was found to be induced in Cu limitation, and to a lesser degree in Fe-limited cells where a Cu-containing Fe oxidase is increasingly expressed (Allen *et al.*, 2007), while genes for Zn transporters respond to Zn

deficiency, and to a lesser degree in Cu deficiency (Supplemental Figure 2). Members of the NRAMP and ZIP family of transporters did not respond to any of these stimuli.
In summary, Ca, P, Fe, Cu, and Zn accumulated in stationary Chlamydomonas cultures; the increase of Ca and P was immediate upon entering stationary growth phase, while the increase of Fe, Cu, and Zn was gradual over time. Fe accumulation was increased with excess supply in the medium, repressing the accumulation of Cu in the process.

Zn and Ca accumulate at higher light intensities, dependent on Fe

The intensity of the light source and the distance of the culture vessel from the light also impacts the quantity of light available to the cell. Besides the direct effect of light on trace metal chemistry (e.g. K_d of FeEDTA is increased due to photo-reductive dissociation (Sunda and Huntsman, 1995)), photon flux density has an impact on gene expression and the abundance of highly-expressed metabolic enzymes (Mettler *et al.*, 2014). We therefore analyzed Chlamydomonas cultures grown at typical laboratory conditions (30, 50, 95, and 180 µmol photon·m^{-2}·s^{-1}, measured inside the culture vessel), with 95 µmol photon·m^{-2}·s^{-1} being the standard light intensity used in our own experiments. In order to avoid any additional influence from changes in the culture density, all cultures were sampled in early logarithmic growth phase (2 – 4 x 10^6 cells/ml). Growth, assessed by doubling time and the number of generations between inoculation and stationary phase (Figure 2 A,B), was not affected in the range of 30 to 180 µmol photon·m^{-2}·s^{-1}. Since growth in the dark under heterotrophic conditions is slow, these results suggest that light serves an additional role to stimulate metabolism rather than as an energy source for photosynthesis. This is supported by the improved growth of many photosynthetic mutants in the presence of light vs. in the dark with acetate (Wang, 1978). The trace element composition is similar in cells cultured at various light intensities, with the notable exception of Zn, which accumulates approximately two-fold at 180 µmol photon·m^{-2}·s^{-1} relative to that measured at our standard set up (Figure 2 C-F). The light-dependent Zn accumulation was repressed when excess Fe was provided in the growth medium (Figure 2 E). Ca levels show a similar trend as Zn, accumulating to ~ 1.5 x at 180 µmol photon·m^{-2}·s^{-1} vs. standard (Figure 2 G) and was also repressed in excess Fe. In fact, even at lower photon flux density, excess Fe reduces the Ca and Zn content of cells (Figure 2 E,G).

While P content was unchanged by the varied PFDs under replete Fe condition, some fluctuations were noted under excess Fe condition (Figure 2 H).

In summary, cellular Zn and Ca levels in Fe replete conditions are affected by changes in light intensity, increasing at higher light intensity, while the stoichiometries of other metals are not impacted by a 5-fold change in photon flux density (representing laboratory illumination). Reduced illumination does not phenocopy the elemental composition in stationary cultures, suggesting that metal accumulation at stationary phase does not result from decreased light penetration.

Fe accumulates, but Ca and P decline in alkaline conditions

The TAP growth medium used in our studies, a popular choice for cultivating *Chlamydomonas reinhardtii* (Harris, 2008), uses Tris/acetate as its major buffer system. In our experiments, the TAP medium is standardly titrated to pH 7 for cultivating cells. As cells assimilate the acetate, the medium becomes more alkaline, reaching ~ pH 8.5 in stationary phase (Figure 3 A). Since pH affects solubility of various ions, changes to the pH can impact metal nutrient availability. We therefore analyzed elemental profiles in cells inoculated in growth media at neutral pH 7 and pH 8.5 under replete and excess Fe conditions. Cultures starting at pH 8.5 reach ~ pH 11 at stationary phase as cells remove acetate from the medium in both Fe replete and excess conditions (Figure 3 A). The rise in pH is dramatic in the starting alkaline medium because the pH falls quickly outside the buffering range of the buffer species (Tris with a pKa of 8.1). Cells in alkaline medium also grew more slowly, with a doubling time of ~ 10 h compared to 8 h in cultures inoculated at pH 7 (Figure 3 B). The growth defect is further exacerbated in excess Fe with a doubling time of ~ 14 h. Nevertheless, the total number of cell divisions between inoculation and stationary phase is unaffected by starting pH or excess Fe (Figure 3 C), indicating that Chlamydomonas acclimates to the more stressful alkaline conditions. Surprisingly, cells experiencing more alkaline conditions accumulated drastically (~ 10 x) more Fe compared to the cells inoculated into the neutral medium (Figure 3 D), and this was further exacerbated in excess Fe (~ 25-30 x). Other trace elements did not differ significantly between cultures inoculated in pH 7 and pH 8.5 (Figure 3 E-G), but Ca and P contents (co-localized predominantly in the acidocalcisomes (Schmollinger *et al.*, 2021) decreased 10-fold (Ca) and 2-fold (P), respectively (Figure 3 H,I).

We noticed a transient increase in the total cellular S content during logarithmic growth in alkaline medium, which was exacerbated in excess Fe (Supplemental Figure 3 A). S is found in proteins and also in glutathione and other metabolites, whose abundances can change due to stress (Lin *et al.*, 2018). Since we used S as a proxy for biomass, we turned to non-purgeable organic carbon content (NPOC) for a direct measure of biomass in these experiments. We noted again a transient increase in carbon (Supplemental Figure 3 B) during logarithmic growth phase, which correlated remarkably well with the cellular S content (Supplemental Figure 3 C). This result points to a transient acclimation period in alkaline medium when cells grow larger (i.e. division inhibited) as opposed to a specific transient overload of S in cellular metabolite pools to combat alkaline-induced proteotoxic conditions. However, the Fe accumulating in these conditions occurs on top of the general increase in biomass, as illustrated by the normalization with S.

In summary, change in pH at stationary phase is not responsible for P, Ca, Cu, and Zn accumulation, while alkaline pH results in Fe over-accumulation and a negative impact on growth rate.

Fe in alkaline conditions is sequestered in acidocalcisomes

We considered the possibility that the measured Fe accumulation at alkaline pH is an artifact of reduced Fe solubility at alkaline pH, resulting in precipitates that are collected with cells and are resistant to solubilization in the EDTA washing steps. To test this, we titrated cell-free TAP medium to pH 8.5, 9.0, 9.5, 10.0, 10.5, and 11.0 and analyzed it for insoluble aggregates by filtration. We did not find significant aggregation of Fe (Supplemental Figure 4 A) up to pH 9.5, but did note aggregation beyond pH 9.5, which could not be reversed by titration back to 7 (Supplemental Figure 4 B).

To distinguish extracellular aggregates from intracellular Fe, we turned to metal-sensitive imaging approaches, which additionally enables the spatial localization of intracellular accumulated Fe. First, we used the Fe(II)-specific fluorescent dye IP1 (Au-Yeung *et al.*, 2013) to visualize Fe(II) in cells inoculated at 8.5, with 20 and 200 µM Fe in the medium (Figure 4 A, Supplemental Figure 5). During logarithmic growth at alkaline pH, we identified quite a few Fe(II) foci intracellularly, mostly near the cell periphery. Cells grown at alkaline pH also showed an increased number of acidic vacuoles relative to those grown at neutral pH, as visualized by LysoSensor DND189 fluorescent dye (pKa ~ 5.1,

Supplemental Figure 6). Taken together, these findings strongly suggested that alkaline-accumulated Fe is sequestered in the P- and Ca-containing acidocalcisomes. We therefore turned to direct elemental imaging of whole cells by X-ray fluorescence microscopy (XFM, Figure 4 B) and to analyzing sections of cells with high spatial resolution nanoscale secondary ion mass spectrometry (NanoSIMS, Figure 4 C,D). Both approaches showed high Fe content within cells grown at alkaline pH, validating the bulk ICP-MS/MS measurements (Figure 3 D) and further showed that Fe, P, and Ca are co-localized, confirming acidocalcisomes as the site of Fe sequestration in high pH medium (Figure 4 B,C, Supplemental Figure 7,8). When we analyzed the intracellular distribution between Ca, P, and Fe content quantitatively, using C to normalize between individual regions of interest, we noted that all 3 elements correlated with each other in alkaline conditions, while only Ca and P were positively correlated, albeit less pronounced, at neutral pH (Figure 4 D).

In summary, we document that Fe in alkaline conditions accumulates in acidocalcisomes towards the periphery of alkaline-grown cells.

Zn levels increased independently of Fe at low temperatures

Depending on the laboratory, standard culture conditions for algae growth can vary between 18-30°C, centered around the 24°C of the standard setup in our laboratory. Cultivation temperature can have a substantial effect on growth, enzyme abundances and consequently trace metal quotas, because of the temperature dependence of chemical reactions (Arcus *et al.*, 2016). For Chlamydomonas, the number of generations between inoculation and stationary phase is constant between 18 and 30°C, but the growth rate below 24°C is reduced significantly (Figure 5 A,B). In terms of elemental profiles, no significant difference was observed with the exception of Zn (Figure 5 C-H). Zn levels increased ~2-fold at 21°C and ~ 3 x at 18°C compared to 24°C (Figure 5 E). This might represent an increased abundance of Zn-containing enzymes at low temperatures to compensate for their reduced enzymatic activity. Unlike at high light intensities, the increase in Zn was not accompanied by an increase in Ca (Figure 2 E,G and Figure 5 E,G) and the amount of Fe in the medium did not affect the amount of accumulated trace metal. We additionally noticed that cellular S levels, which we used for normalization, decreased subtly but non-significantly as temperature increased (Supplemental Figure 9

A). We therefore additionally analyzed the elemental composition on a per-cell basis and determined the amount of cellular carbon (Supplemental Figure 9 B). Correlation of total cellular S and C content showed again a subtle decline in S with respect to relatively unchanged biomass as cultivation temperature increased (Supplemental Figure 9 C). Interestingly, trace element, Ca and P abundance, similar to S, also showed a subtle, gradual decline as the cultivation temperature increased, most noticeably from 24 to 30°C, but again the differences were not significant with respect to the reference cells at 24°C (Supplemental Figure 9 D-I).

Overall, Zn content is elevated at low cultivation temperatures, independently of medium Fe concentration, while the total amount of cellular trace elements, Ca, P, and S is subtly reduced as the environment warms.

The impact of aeration on elemental profiles

Photosynthetic microorganisms grown in liquid growth medium utilize dissolved CO_2 for photosynthetically-driven carbon assimilation. Limitations in CO_2 supply induce acclimation responses to low-CO_2 environments, potentially affecting growth or the trace element quota of cells, for example by changes in abundance of Zn-containing carbonic anhydrases or the Fe-rich photosynthetic complexes (Moroney *et al.*, 2011, Huang *et al.*, 2021). In laboratory growth setups, agitating flasks to facilitate gas exchange between the growth medium and the adjacent air or bubbling cultures with air (with or without additional CO_2) are commonly utilized to avoid CO_2 limitation of photosynthesis (or O_2-limitation for respiratory growth). Aeration can also affect the speciation of redox active trace metals like Fe and Cu with Fe species becoming less soluble and Cu species becoming more soluble and more bio-available.

In order to study the influence of aeration, we manipulated the culture setup as is common in the laboratory to lower the efficiency of gas exchange, either by reducing shaker speed, increasing fill-levels of the growth vessels, or altering the flask size and type. We reduced the speed of agitation from 180 RPM in the standard setup to 160, 140, 120, 60, and 0 RPM. At 0 and 60 RPM, cells settled to the bottom of the flask, but this did not affect the number of divisions between inoculation and stationary phase and only marginally affected the growth rate (Figure 6 A,B). Interestingly, the cultures that were agitated poorly (0, 60 RPM) had doubling times that were slightly, albeit non-significantly, improved,

relative to those that were heavily agitated (120-180 RPM), suggesting that gas exchange rate is not growth-limiting in photoheterotrophic conditions.

Elemental analysis showed that the Fe storage capacity was not affected by agitation (Figure 6 C). However, a ~ 2 x increase in the Cu content was observed in cultures with no or minimal agitation (0, 60 RPM, Figure 6 D). This increase in Cu, in contrast to the situation in stationary cells, was not dependent on the Fe content of the growth medium, and it may reflect the increased expression of the nutritional Cu regulon (including assimilatory Cu transporters) by hypoxia (Hemschemeier *et al.*, 2013). Zn and P did not change (Figure 6 E,H), but we noted a subtle, significant increase for Mn (1.2 x) and a subtle decrease of Ca under poor agitation (0.8 x), only when excess Fe was present (Figure 6 F,G).

When we adjusted the fill-level of the Erlenmeyer flasks between 10 and 80%, deviating from the 40% (100 ml growth medium in 250 ml Erlenmeyer flask) used in the remainder of the study, doubling times increased by ~ 1.5 h in flasks with growth medium equivalent to 60% or more of the flask's volume (Figure 7 A). Yet, compared to the standard 40% fill-level, the growth rate did not improve at reduced fill-levels (20% and below), indicating that 40% is an optimum level in the laboratory. The number of generations between inoculation and stationary phase was not affected (Figure 7 B B). ICP-MS/MS analysis indicated similar amounts of Fe, Cu and Zn between cultures with 10 to 80% fill-fraction of culture-to-flask volume (Figure 7 C,D,E). Compared to the reference conditions, Mn, Ca, and P contents were reduced by ~ 25% when the fill-fraction was 20% or below (Figure 7 F,G,H). Excess Fe in the medium restored the P quota to abundances observed at 40% fill-level or higher (Figure 7 H), but the Mn quota was still significantly reduced in Fe-excess conditions (Figure 7 F). Ca level showed increased variance at lower fill-levels, which appear to be a slight, non-significant reduction (Figure 7 G).

We also altered the size and type of the culture vessel between 125-2800 ml, here again filling each of them to 40% of the vessel capacity and shaking the cultures at 180 RPM. Erlenmeyer flasks were used from 125- to 1000-ml capacity, while Fernbach flasks were used for 2800-ml capacity (Supplemental Figure 10). Growth, as well as elemental composition and Fe storage capacity, were quite stable when only the vessel was changed, indicating that when the fill-level and agitation speed is kept constant, the cells do not experience any change in aeration efficiency.

In summary, Cu, Mn, Ca, and P quotas are affected when aeration efficiency is altered by changing shaker speed or fill-levels of the growth vessels, with the trace element quotas not being affected by the Fe content of the medium.

CC-1690 and CC-1691 have a reduced Ca quota, while CC-1691 accumulates Cu

Chlamydomonas reinhardtii has been a subject of laboratory research for decades. All the strains presently used in research were derived from Gilbert Smith's original isolation of Chlamydomonas in Massachusetts in 1945 (Harris, 2008, Gallaher *et al.*, 2015). A recent survey of laboratory wild-type strains has demonstrated considerable genetic diversity among 39 commonly used laboratories strains (Gallaher *et al.*, 2015), attributable to two alternate haplotypes, which were proposed to be derived from an ancestral cross between parental strains with ~2% relative divergence. We compared seven Chlamydomonas wild-type strains with respect to their growth, elemental composition, and capacity to store Fe. These seven strains include CC-4533, which is used throughout this study and is used as the parental strain of the Chlamydomonas insertional mutant collection (Li *et al.*, 2019); CC-4532, which has been widely used for trace element studies in the alga (Blaby-Haas and Merchant, 2012, Merchant and Helmann, 2012); and five additional strains, each representing a distinct Chlamydomonas lineage with a unique haplotype pattern (Gallaher *et al.*, 2015). All strains grew well in our setup at similar rates and produced the same number of generations, independent of medium Fe concentration (Figure 8 A,B). Compared to CC-4533, we found only a few significant differences in the elemental composition between the strains: CC-1690 contained ~ 20% less Fe (Figure 8 C); the Zn quota in CC-1009 is ~25% reduced (Figure 8 E), and CC-1691 showed a ~ 1.5 x higher Cu content than the other tested strains (Figure 8 D). The Fe storage capacity was not significantly different between the tested strains (Figure 8 C). Mn and P levels in all strains were maintained in a similar range (Figure 8 F,H), but CC-1690 and CC-1691 both had ~40% less Ca (Figure 8 G,). Altogether, CC-1690 and CC-1691 were most different among the tested strains, with the most prominent changes affecting the Ca and Cu quota.

Changes in elemental composition alone are sufficient to identify and distinguish the cultivation condition

We systematically analyzed the influence of changes to temperature, pH, culture density, light intensity and aeration in otherwise strictly controlled culture conditions on the ionome of Chlamydomonas cells. During these experiments, we identified specific modifications to the elemental quota upon many of the studied perturbations. In order to identify common and specific modifications to the cellular elemental quotas we performed a global principal component analysis of all experiments described here (Figure 9), and also for each individual experiment (Supplemental Figure 11). Most samples group together nicely with the default growth mode (pH 7, 80-95 PAR, 24°C, 180 rpm at 40% fill level in a 250ml Erlenmeyer flask). Several groups however separate from the bulk of the samples, most prominently the samples at pH 8.5, both in 20 and 200 µM Fe. These cultures distinguish themselves with a highly elevated Fe content and reduced Ca and P content (Figure 3 D,H,I). Additionally, a bigger group clearly separates from the bulk of the samples, containing all the cultures sampled in stationary conditions (Figure 9). These cultures originate from two experiments, at different times in stationary phase (Figure 1 B) and at different temperatures in stationary conditions (Supplemental Figure 9 A-C). These cultures had elevated Fe, Cu, Zn, as well as P and Ca content then cultures sampled during logarithmic growth (Figure 1 E-G,I,J). The elemental composition of cultures at 75h, right at the onset of stationary phase (Figure 1B), are positioned right in between the group of stationary and logarithmic cultures (Figure 9). Closer to the main group, additional separation can be found for cultures grown with lower fill levels (10 and 20%); probably due to lower P, Ca and Mn levels. The cultures grown at 30°C, 180 PAR and in 2.8; Fernbach flasks can also be distinguished, albeit the separation is not as pronounced as with the other conditions.

Taken together, elemental quotas alone can be indicative of the conditions that the cultures were grown in, and individual elemental signatures allow to determine the growth status of the cultures.

Discussion

We set out to systematically analyze the consequences of typical laboratory variations in cultivating conditions to the rate and extent of Chlamydomonas cell growth, the trace element quota, and macronutrients P, S, and Ca content. We identified several changes that affected the growth rate, but none affected the number of generations between inoculation and stationary phase. This indicates that typical laboratory perturbations do not limit growth but rather may induce an acclimation response that either temporarily or in a sustained way affects the rate of growth (or doubling time). We typically did note a change in the elemental composition of the cells in response to most of the subtle changes in culture conditions or in between different wild-type strains, and interestingly, most of these changes were unique and specific to the altered variable. This highlights the necessity of a detailed documentation of growth conditions for any kind of experiment, especially the recording of secondary parameters that were not the direct target of the study, like cell density at sampling, light intensity/quality, medium pH, vessel properties and shaker settings, to facilitate the generation of reproducible results across laboratories, or even in the same laboratory, in between individual experiments, experimentalists or growth chambers.

Because of the impact of Fe limitation on primary productivity and our interest in mechanisms for handling fluctuation in Fe bioavailability, we also used replete (20 µM) vs. excess (10x, 200 µM) Fe as a variable. We discovered two scenarios for Fe over-accumulation: stationary phase and alkaline growth. In both situations, cells already displayed higher Fe accumulation in the replete Fe condition (Figure 1 E, Figure 3 D), but further increased intracellular Fe in response to excess external Fe. Excess Fe in the growth medium in some cases could also impact intracellular P and Ca, or other trace elements, either increasing or reducing their abundance, depending on the specific perturbation. This is further evidence of the interconnection of trace metal metabolism; replacing specific trace-metal dependent cellular functions by alternate means, adjusting to the (bio-)availability of nutrients in the respective environment, or avoiding protein mis-metalation.

Accumulation of nutrients in stationary phase, deliberate or accident?

Fe, Cu and Zn accumulate linearly over time in stationary Chlamydomonas cells, suggesting continued uptake of these elements even when cells have stopped dividing. For Fe, this had been observed already in *S. cerevisiae*, which had also been found to accumulate Fe linearly with time during post-exponential growth (Park *et al.*, 2013). The authors therein hypothesized that, in addition to low affinity uptake systems, which do not respond to growth rate, the high-affinity Fe import pathway in *S. cerevisiae* turns off more slowly than the rate of cell growth declines, causing cells to continue Fe import during stationary growth and hence over-accumulate Fe. However, we did not observe a decline in the rate of accumulation even after three days (equivalent to ~ nine generations during log phase); the relationship was linear throughout that time period. This suggests also that the transporters for these metals are stable on the plasma membrane at stationary phase. A proteomic comparison of log vs. stationary phase cells would be interesting in that context.

Fe is prone to scarcity in nature and a limiting factor for growth, in general for all but especially for photosynthetic organisms (Morel *et al.*, 1991, Behrenfeld *et al.*, 2009). Thus, it is possible that organisms have evolved to deliberately allow a moderate over-accumulation of Fe. In a previous study, we found the intracellular Fe concentration, outside of the cytosolic storage vacuoles, to be stable in situations of transient hyper-accumulation (Schmollinger *et al.*, 2021). This was similarly predicted in simulations in yeast (Park *et al.*, 2013) and could explain the mechanism for continued uptake. Cells might allow additional Fe uptake via low and high affinity uptake systems until storage sites are saturated and the cytosolic, non-sequestered Fe concentration starts to increase. Cu and Zn accumulation followed the same kinetic behavior in stationary phase, a continuous accumulation over a period of time equivalent to multiple generations during log phase. Furthermore, it was interesting to observe that the Cu accumulation in stationary cells was reduced when excess Fe was provided in the growth medium and, instead, more Fe was accumulated. In Fe-excess medium, Cu and Fe still accumulated at a constant rate during stationary phase, but the rates were altered, with that for Fe being increased and Cu being reduced. Whether this is a consequence of Fe nutrition impacting the expression of Cu transporters needs to be experimentally tested.

Both Fe and Cu share the same sequestration site in hyper-accumulating conditions (Hong-Hermesdorf *et al.*, 2014, Schmollinger *et al.*, 2021), thus limited capacity for the combined amounts of Cu and Fe could explain the observed change in uptake dynamics. The sequestration site for accumulating Zn is yet to be identified in Chlamydomonas. However, its accumulation was unaffected by the Fe concentration in the medium. In this context, it was interesting to note an increase in cellular Ca and P content in stationary conditions. It was shown previously in quick-freeze deep-etch electron microscopy images that acidocalcisomes were accumulated in Chlamydomonas cells collected from stationary phase, but not in cells from log phase (Goodenough *et al.*, 2019). This result indicates that the accumulation of Ca and P in stationary cells might correlate with an increased abundance of the storage organelles, facilitating safe transition metal sequestration. Curiously, Mn did not follow the same pattern as Fe, Cu, and Zn; cellular Mn content remained relatively constant from log to stationary phase, even though Mn can be sequestered in acidocalcisomes (Tsednee *et al.*, 2019). Again, assessment of the abundance and activity of Mn assimilation transporters in log vs. stationary phase might explain the discrepancy. Nevertheless, these transporters and mechanisms have not yet been definitively identified.

A counterintuitive role of pH in metal accumulation

Photoheterotrophic growth of Chlamydomonas into stationary phase involves medium alkalinization from acetate assimilation, and a reduction of the perceived photon flux density (PFD) in the culture from the increased cell density. We aimed to uncouple both of these components from stationary phase conditions by analyzing their influence separately by other means. The elemental composition in cultures grown directly in more alkaline growth medium and in reduced PFD was quite different from the elemental profile in stationary cells, making it unlikely that the observed changes to the quotas in stationary cells were the results of either or a combination thereof. Stationary phase cultures suffer from decreased light availability to individual cells because of shading effects at high cell densities (Figure 1 A). None of the elements that accumulated in stationary phase (Fe, Cu, Zn, P, Ca) accumulated also at lower PFD. On the contrary, Zn and Ca showed the opposite behavior and accumulated at higher PFD, while other elements were unchanged. In alkaline conditions, Cu and Zn did not accumulate, and P and Ca abundance was

reduced, again showing the opposite behavior compared to stationary cultures. Fe was the only element that did accumulate in alkaline conditions, but to a much higher degree than observed in stationary conditions. Therefore, it is possible that the Fe accumulation component of stationary phase cultures is partially caused by medium alkalinization. The overall elemental signature in alkaline conditions and the extent of accumulation, however, is clearly distinct.

The specific over-accumulation of Fe in cells grown in alkaline medium is intriguing and counter-intuitive, because alkaline pH reduces Fe solubility and lowers Fe bioavailability in the environment as well as in laboratory growth medium, by raising the K_d of FeEDTA, which is used to deliver the Fe (Sunda and Huntsman, 2003). Plants grown in alkaline soil can become chlorotic and stay small due to Fe deficiency (Mengel and Geurtzen, 1986, Kim *et al.*, 2006). One explicit strategy to improve Fe acquisition in plants is to increase Fe solubility by soil acidification. By inducing outward proton fluxes via plasma membrane ATPases, non-grass plants improve Fe acquisition in alkaline environment (Römheld *et al.*, 1984, Santi and Schmidt, 2009). Similarly, studies have shown that *S. cerevisiae* has a greater tolerance for alkaline stress either when Fe importers are over-expressed, or jwhen additional Fe is supplied in the growth medium (Serrano *et al.*, 2004, Serra-Cardona *et al.*, 2015), indicating that Fe-limitation may be a contributing factor to growth defects in alkaline conditions. While the growth rate was reduced in alkaline conditions in Chlamydomonas cultures, it was most likely not due to Fe limitation. First, providing additional dissolved Fe, as in the yeast case, did not improve the growth defect; the opposite was the case, the growth rate declined further (Figure 3 B). Second, the amount of cell-associated Fe was already increased in alkaline conditions, which was further exacerbated with more Fe (Figure 3 D). Fe in the growth medium was still soluble for the most part of the cells' growth phase; and even when the medium pH reached pH 11, a considerable portion of the Fe pool was still found in solution (Supplemental Figure 4), well above the amounts provided in replete conditions. Chlorosis, another indicator of Fe deficiency commonly present in alkaline-soil grown plants, was also not observed in alkaline-grown Chlamydomonas cells (Kim *et al.*, 2006). Lastly, the location of the Fe foci at the cell periphery might be an indication that the accumulated excess Fe was on the path to be expelled by the cells to prevent toxicity, rather than being used or stored for future use. From both XFM and NanoSIMS imaging, we noted Fe co-localized with P and

Ca in the periplasm of cells. Studies have identified heavy metals in the polyP granules of yeast, fungi, algae and bacteria, and have linked polyP degradation and phosphate efflux to detoxification of the heavy metals (Keasling, 1997, Docampo, 2006, Lavoie *et al.*, 2009). Despite the accumulation of intracellular Fe in alkaline condition, Ca and P contents in Chlamydomonas cells were reduced. A substantial fraction of the cellular P and most of the intracellular Ca are found within acidocalcisomes in Chlamydomonas (Schmollinger *et al.*, 2021), which were still the sites for Fe sequestration in alkaline conditions.

It is worth noting that a reduced content of Ca and P does not preclude the formation of acidocalcisomes and their use as a storage site for Fe. In the Chlamydomonas *vtc1* mutant strain, which fails to accumulate P and Ca in acidocalcisomes, acidic compartments have still been observed and accumulated Fe was still sequestered there, in a similar manner to that in the corresponding wild-type strains (Tsednee *et al.*, 2019, Schmollinger *et al.*, 2021). Likewise, we still found acidic compartments using LysoSensor in this study, increasingly more so in alkaline conditions (Supplemental Figure 6). Co-localization analyzed by NanoSIMS and XFM showed a good correlation between Fe, Ca and P, despite the lower total cellular abundance of Ca and P. We did however note that, compared to Fe over-accumulation following Fe-limitation (Schmollinger *et al.*, 2021), co-localization with P in alkaline conditions was less pronounced.

Interestingly, while acidic bodies, detected by LysoSensor, were observed throughout the alkaline pH-grown cells, the Fe/Ca/P foci seen in NanoSIMS and XFM images were mostly observed around the periplasmic space of the cells (Supplemental Figure 7,8 Figure 4 B,C). Similarly, the Fe(II) foci detected through IP1 were mainly found in the peripheral region (Figure 4 A, Supplemental Figure 5). LysoSensor additionally detected acidic vacuoles also in cultures inoculated into neutral growth media that we were not able to identify with the elemental techniques. We speculate that a portion of the population of acidocalcisomes is not used for metal sequestration, but for a more general function, such as pH homeostasis. Exposure to high external pH might cause a general imbalance of intracellular protons and/or other cations, disturbing the biochemistry that is required for functional transport of Ca or P.

The formation of acidic bodies in alkaline-grown cultures may be helpful for balancing these proton gradients, in addition to housing overloaded Fe. Degradation of polyP in alkaline conditions has been described in *S. cerevisiae* (Castro *et al.*, 1995, Serra-

Cardona *et al.*, 2015). In yeast, the vacuolar H^+-ATPase (V-ATPase) is a crucial component of pH homeostasis (Serrano *et al.*, 2004, Martínez-Muñoz and Kane, 2008), which is required for generating a well-balanced proton gradient and enables efficient uptake of different nutrients (Ariño *et al.*, 2010). In particular, it has been shown that a higher extracellular pH stabilizes the V-ATPase complex, making it less susceptible to dissociation and increasing its activity (Serrano *et al.*, 2004, Padilla-López and Pearce, 2006). Mutants lacking structural or assembling components of the V-ATPase were more sensitive to even moderate alkalinization of the growth medium (Serrano *et al.*, 2004, Ariño *et al.*, 2010). Thus, functional acidic vacuoles may play a similar role for alkaline pH tolerance in Chlamydomonas.

Abiotic parameters effecting elemental composition

Earlier studies had reported changes in trace metal metabolism of photosynthetic organisms in response to variations in light intensity (Long and Merchant, 2008, Rodriguez and Ho, 2017). In the majority of studies, the light intensities investigated were used to analyze either low or high light stress in cultures, which is often accompanied by additional perturbations like the additional production of ROS. For example, in Chlamydomonas, increasing the light intensity to 500 PFD did not affect the cellular Fe quota, despite a number of important components of the Fe uptake machinery (FOX1, FRE1, FEA1) being severely reduced both at the RNA and protein level (Long and Merchant, 2008). The dinoflagellate Symbiodinium showed improved acclimation to higher light intensities (~670 PFD) when additional Fe was provided to cells; the respective quotas thereby were also increased (Rodriguez and Ho, 2017). Mettler and colleagues studied a transition within a similar light intensity range (from ~40 to ~140 PFD) as in this work, in a well-controlled Chlamydomonas bioreactor system that showed changes in metabolite and protein abundances (*e.g.* those involved in photosynthesis), indicating that even within a physiological range of light intensities, acclimation is taking place and also affecting metal-utilizing enzymes (Mettler *et al.*, 2014). Carbonic anhydrase 1 (CAH1), an abundant Zn-containing protein involved in carbon concentration, was accumulated in the higher light intensity experiment, while ribosomes, another major Zn sink in cells, were shown to be reduced both in organelles and the cytosol (Mettler *et al.*, 2014). We noted a marked increase in Zn content and Ca, which was prevented when excess Fe was provided. We

did not note any adverse effect on growth, but high amounts of Fe together with higher light intensities, while individually not deleterious, can result in cell damage or even cell death (Long and Merchant, 2008).

Temperature affected the growth rate, mostly in predictable ways. Chlamydomonas had been reported to grow optimally between 20-25°C (Harris, 2008). We noted markedly slower growth at 21ºC and below, but quite similar growth rates from 24 up to 30ºC. The reduced growth rate at low temperatures was accompanied with elevated Zn levels. In Arabidopsis, shifts to lower temperatures (10°C) than the ones used in our study (18/21°C) were shown to involve upregulation of cytosolic ribosomal proteins (Beine-Golovchuk *et al.*, 2018), which could potentially explain the requirement for more Zn in these conditions. An increase in temperature was accompanied with an overall, slight reduction of trace element, S, P and Ca content per cell, with exception of the total C content. This could generally indicate that with an increase in enzymatic efficiency at elevated temperatures, there may be lower requirements for metal-requiring protein/enzyme content in general (as indicated by the S content) and less requirements for storage sites like vacuoles (as indicated from P, Ca reduction). Studies have shown that in various algal species, including *C. reinhardtii*, increasing cultivation temperature results in modulation of the fatty acid profile, which is not reflected in the total cellular C content, and lipid accumulation, which might contribute to maintaining the C content specifically (James *et al.*, 2013, Lukeš *et al.*, 2014, Morales-Sánchez *et al.*, 2020, Li *et al.*, 2021).

Conclusion

Subtle changes to otherwise strictly controlled growth conditions of incubator-grown algae affect the (trace) elemental makeup of the cultures in specific ways. Individual changes to the elemental quota alone allow one to distinguish individual growth conditions. Most prominently we identified increased Fe, Cu and Zn storage during stationary phase, and severe Fe accumulation in alkaline-grown cultures, which is intracellularly sequestered in acidocalcisomes.

Material and Methods

Strains and culturing conditions

Chlamydomonas reinhardtii strain CC-4533 (wild-type, *cw15*, *mt-*) was used for all experiments presented in this study. When analyzing the diversity among laboratory strains, CC-4533 was compared with six other wild-type strains, including CC-4532, CC-124, CC-125, CC-1009, CC-1690, and CC-1691, all obtained from the Chlamydomonas Resource Center (http://chlamycollection.org/). Unless specified otherwise, the alga was grown in tris-acetate-phosphate (TAP) medium developed by Gorman and Levine (Gorman and Levine, 1965, Harris, 2008), utilizing a revised mineral nutrient supplement according to Kropat (Kropat *et al.*, 2011) to provide optimized amounts of trace elements instead of Hutner's trace element mixture (Hutner *et al.*, 1950). Within most experiments presented here, the Fe supplement (Supplement 6 in Kropat's revised mineral supplement suite) was provided at replete (1x, 20 µM) or excess (10x, 200 µM) concentration. Unless specified otherwise, cells were inoculated at 1 x 10^4 cells/ml in 100 ml growth medium in a 250-ml Erlenmeyer flask, titrated to pH 7.0 with trace metal grade acetic acid (Fisher, A507-P212) and KOH. Cells were inoculated from a liquid pre-growth culture during logarithmic growth phase (1 – 4 x 10^6 cells/ml) grown in TAP growth medium with 20 µM Fe. The cultures were grown in an Innova 44R incubator (New Brunswick Scientific) at 24ºC under constant agitation at 180 RPM and continuous illumination at 80-95 µmol photons·m^{-2}·s^{-1}. Photon flux density (PFD) was measured inside a separate cell-free TAP medium Erlenmyer flask. The incubators were equipped with six cool white fluorescent bulbs at 4,100 K and three warm white fluorescent bulbs at 3,000 K. The light quality spectrum (Supplemental Figure 12) inside the incubator was recorded using a PSI SpectraPen (Photon Systems Instruments). For all experiments, three independent cultures were inoculated and grown in parallel in random positions in the incubator in the central area with comparable PFD. Cells in each culture were counted manually using a hemocytometer. A 1-ml aliquot of each culture was sampled, thoroughly mixed, and treated with 3-10 µL of iodine solution (0.25 g iodine in 100 mL 95% EtOH), depending on cell density, to stain and immobilize cells. 10 µL of the stained cells were loaded into the counting chamber of the hemocytometer. At high cell densities, the mixture was further diluted with TAP medium, to ensure accurate readouts. Doubling time was calculated

between consecutive time points using $k = t\log(2)/(\log(O_t) - \log(O_0))$, where k is the doubling time, t is the time between the measurements, and O_t and O_0 are the culture densities at the time of measurement. The number of generations from time of inoculation until stationary growth phase was calculated using $n = \log(O_f/O_0)/\log(2)$, where n is the number of generations, O_f is cell density in stationary conditions, and O_0 is the cell density at inoculation.

Quantitative elemental composition analysis (ICP MS/MS)

Trace metal abundance including Fe, Cu, Zn and Mn, as well as the abundances of macronutrients S, Ca and P were determined by ICP-MS/MS as described in (Strenkert *et al.*, 2016) with minor modifications. Briefly, 5 x 10^7 cells were collected by centrifugation at room temperature at 2,600 x *g* for 3 min in a 50-ml Falcon tube (Eppendorf 5810R). 2 ml spent medium were collected from the supernatant of this centrifugation step, diluted to 7 ml with Milli-Q water containing Optima grade nitric acid (Fisher, A467-500, final concentration 2% nitric acid). The cell pellets were washed twice with 1 mM Na_2-EDTA to remove cell surface-associated metals and once with Milli-Q water. The washed cell pellet was overlaid with 143 µl of 70% nitric acid (Optima grade, Fisher, A467-500) and digested at room temperature overnight, followed by a 2-4 h incubation at 65ºC. The cell hydrolysate was diluted to 5 ml with Milli-Q water (final nitric acid concentration of 2%). Fe, Cu, Zn, Mn, S, Ca, and P contents in the spent media and cell lysates were measured by ICP-MS/MS on an Agilent 8800 or Agilent 8900 instrument in three to five technical replicates. The average variation between the technical replicate measurements was below 2% for all analytes and never exceeded 5% for an individual sample. A dilution series of an environmental calibration standard (Agilent 5183-4688), a sulfur (Inorganic Ventures CGS1) and a phosphorus (Inorganic Ventures CGP1) standard was used for quantification. ^{45}Sc and ^{89}Y were used as internal standards (Inorganic Ventures MSY-100PPM, MSSC-100PPM) to account for sample composition differences between standards and cell lysates. The total content of all analytes in the samples was determined in MS/MS mode: ^{40}Ca and ^{56}Fe were determined directly using H_2 as a cell gas, whereas ^{55}Mn, ^{63}Cu, and ^{66}Zn were measured using He in the collision cell, and ^{31}P and ^{32}S were determined via mass-shift from 31 to 47 and 32 to 48, respectively, using O_2 as a cell gas. The data was first analyzed with Masshunter (Agilent, v4.4) and further in Microsoft Excel

and OriginPro 9.1 (OriginLab). Trace metal, Ca and P contents were normalized to the total S content if cellular S content correlated linearly with cell number and total organic carbon (TOC) content and was within a similar range across the experiment (Supplemental Figure 2). The cell number was used instead if that was not the case.

Quantitative total organic carbon analysis (NPOC)

Total, non-purgeable organic carbon content of the cells was determined from ICP lysates on a Shimadzu TOC-L/TN CSH analyzer. Briefly, 500 µl of the digested cell lysates, prepared and used for ICP-MS/MS as described above, were subsequently diluted with 14.37 ml of Milli-Q water and 135 µl of 3 M HCl (to a final HCl concentration of 27 mM, and final nitric acid concentration of 0.067 %). 2% nitric acid was diluted likewise and used as a blank. Samples were sparged with purified air. A standard curve from 0.5 to 25 ppm carbon from a Potassium Hydrogen Phthalate standard was used for quantification. The data was analyzed in the TOC control software (Shimadzu), Microsoft Excel and OriginPro 9.1 (OriginLab).

Principal components analysis

To summarize the effects of different environmental perturbations several principal component analyses (PCA) were performed, using the princomp function in R. The data was scaled and centered around the mean for each individual element (z-scores). The cellular content of seven elements was used in these calculations: P, S, Ca, Mn, Fe, Cu and Zn.

TAP medium titrations

To assess pH-dependent Fe precipitation in TAP medium, a flask of fresh TAP medium with 200 µM Fe was prepared and titrated to 8.5, 9.0, 9.5, 10.0, 10.5, and 11.0 with KOH. In the reverse direction, to assess whether any Fe precipitate could be re-solubilized in acidified medium, fresh TAP medium at pH 11.0 was titrated to pH 10.5, 10.0, 9.5, 9.0, and 8.5 with acetic acid. The media were left undisturbed at each titration point for 30 mins at room temperature before 4 ml of each were collected, of which 2 ml was filtered through a 0.22 µm filter to remove insoluble material. Both the filtered and unfiltered samples were analyzed, as described above, by ICP-MS/MS to evaluate their Fe content.

Laser scanning confocal microscopy

4 x 10^6 Chlamydomonas cells were collected by gentle centrifugation (2,600 x *g* for 1 min) and washed twice with 10 mM sodium phosphate buffer (pH 7.0), before being resuspended in 50 µl of the diluted fluorescent dyes. Both dyes, LysoSensor DND189 (Thermo Fisher Scientific) and IP1, custom made according to (Au-Yeung *et al.*, 2013), were diluted in 10 mM sodium phosphate (pH 7.0) to a final concentration of 2 µM (LysoSensor) or 200 µM (IP1). Cells were mounted on glass slides for laser scanning confocal microscopy. For imaging of LysoSensor-stained cells, images were captured on a Zeiss LSCM Airyscan 880 equipped with a X63/1.4 oil immersion objective in channel mode. Imaging of IP1-stained cells was performed on a LSM880 with a X63/1.4 oil immersion objective. Exposure time, fluorescent emission signals from the dyes and chlorophyll, and all other imaging controls were adjusted via the Zeiss ZEN Black software.

NanoSIMS

Samples collected for NanoSIMS were chemically fixed prior to embedding into resin and sectioning. Cells were collected from each culture by gentle centrifugation at 2,600 x *g* for 1 min. The resulting cell pellets were washed once with 1 mM Na_2-EDTA to remove cell-associated trace elements and twice with 10 mM sodium phosphate (pH 7.0), before fixation in 2% glutaraldehyde and 2% paraformaldehyde in 10 mM sodium phosphate (pH 7.0) overnight at 4ºC. The fixed samples were rinsed three times, 10 min each, with 0.1 M sodium cacodylate (pH 7.2) and stained post-fixation with 1% OsO_4 in 0.1 M sodium cacodylate (pH 7.2) at room temperature for 1 h. After rinsing again with sodium cacodylate, samples were dehydrated stepwise with acetone (35, 50, 70, 80, 95, 100, 100, 100%) for 10 min each. The dehydrated samples were infiltrated with Epon-Araldite resin, sequentially reducing the acetone fraction, 30 min each, using 2:1, 1:1, 1:2 acetone : resin mixtures, before pure resin was used, first for 30 min, then for 1h and finally for 2h. The infiltrated samples were then embedded in fresh pure resin and cured at 60ºC for 48 h. Sections of 200 nm thickness were cut on an ultramicrotome (Leica EM UC6) using a diamond knife before being deposited on 200-mesh carbon- and Formvar-coated copper grids. Sections were post-stained with 1% uranyl acetate for 4 min and lead citrate for 2

min. The samples were analyzed in a CAMECA NanoSIMS 50 (Gennevilliers, France) at Lawrence Livermore National Laboratory (LLNL) to determine intracellular elemental distributions, as described previously (Tsednee *et al.*, 2019). Briefly, a primary oxygen ion beam in scan mode was focused on each specific region of the section to generate secondary ions, which were subsequently analyzed in a mass-spectrometer. The MS was tuned to ~3,500 mass resolving power, and $^{12}C^+$, $^{31}P^+$, $^{40}Ca^+$, and $^{56}Fe^+$ were detected simultaneously in pulse counting mode using electron multipliers. The peaks for the elements were identified using a calibration from NBS 610 glass (National Institute of Standards and Technology, USA). The analysis areas were pre-sputtered at high current (~1.2 nA O^-) to establish sputtering equilibrium, before either a region with multiple cells was scanned at ~400 nm spatial resolution (100 pA O^-, 40 x 40 μm^2 raster, 256 x 256 pixels, 1 ms/pixel, 30 cycles) or an individual cell at 150nm spatial resolution (30 pA O^-, 15 x 15 μm^2 raster, 256 x 256 pixels, 1 ms/pixel, 25 cycles). The samples were additionally imaged on a transmission electron microscope (FEI Tecnai TEM at UC Berkeley Electron Microscope Lab) and/or a scanning electron microscope (FEI Inspect F FEG-SEM at LLNL) before and after the NanoSIMS analyses to obtain the correlated images of cell structures. The NanoSIMS data were quantitatively analyzed using custom software (L'Image, L.R. Nittler, Carnegie Institution for Science, Washington, D.C.). The images were corrected for detector dead time (44 s), before the final images were produced. Regions of interest (ROIs) were defined using an automated algorithm that subdivided the analyzed area into same-sized regions. Regions that did not contain cells were manually deleted. Ion ratios ($^{31}P/^{12}C$, $^{40}Ca/^{12}C$, and $^{56}Fe/^{12}C$) were calculated for each ROI by averaging the ratios over replicate scans. Because the NanoSIMS data were not standardized by a matching standard, concentrations could not be deduced.

X-ray fluorescence microscopy

Samples for X-ray fluorescence microscopy were prepared as described previously (Schmollinger *et al.*, 2021) with minor modifications. Briefly, 3 x 10^6 cells were collected from cultures by quick centrifugation (16,100 x *g* for 15 s). The resulting cell pellets were washed twice in 1 x phosphate-buffered saline (PBS) buffer (137 mM NaCl, 2.7 mM KCl, 10 mM Na_2HPO_4, 1.8 mM KH_2PO_4) and fixed in 4% paraformaldehyde in PBS at room temperature for 10 mins. Then, 100 µl of the fixed cell suspension were spotted onto a

poly-L-lysine-coated silicon nitride window (5 x 5 x 0.2 mm frame, 2 x 2 x 0.0005 mm Si_3N_4 membrane, Silson) and allowed to settle for 30 mins. Residual supernatant on the windows was removed by gentle suction and the windows were subsequently washed twice with PBS, once using fresh 0.1 M ammonium acetate, and once with Milli-Q water. The windows were air dried over night at room temperature. The samples were analyzed at the Bionanoprobe at ANL's Advance Photon Source (Lemont, IL) (Chen *et al.*, 2014). The incident X-ray energy was tuned to 10 keV to aim for direct excitation of atomic K transitions of elements up to z = 30 (Zn). Two coarse scans were performed to identify the coordination of cells on the windows, followed by a high-resolution scan for each cell (~90 nm step size). Data were fitted and analyzed using the MAPS software package (Vogt, 2013).

Data availability statement

All relevant data can be found within the manuscript and its supporting materials.

Acknowledgments

This work was supported by a Department of Energy grant DE-SC0020627 (to S.S.M. and S.S.). Colleen Hui was supported by the Graduate Research Scholar Program at Lawrence Livermore National Laboratory. This research used resources of the Advanced Photon Source, a U.S. Department of Energy (DOE) Office of Science User Facility, operated for the DOE Office of Science by Argonne National Laboratory under Contract No. DE-AC02-06CH11357. We appreciate the support of Keith Brister and Michael Bolbat at 21-ID-D and the support of Evan Maxey at 9-ID-B of the APS. Work at Lawrence Livermore National Laboratory is supported by US Department of Energy Office of Science, Genomic Science Program under contract SCW1039 and was performed under the auspices of DOE contract DE-AC52-07NA27344. Confocal microscopy experiments were conducted using a Zeiss LSM 880 with OPO, at the CRL Molecular Imaging Center, supported by the Helen Wills Neuroscience Institute. We would like to thank Alison Frand, Holly Aaron and Feather Ives for the training and assistance at the microscopes. We also want to thank the group of Chris Chang at UC Berkeley for providing assistance in producing the fluorescent dye IP1. We thank the staff at UC Berkeley Electron Microscope Lab for advice and assistance in the sample preparation for NanoSIMS and EM. The authors declare no conflict of interest.

Author contributions

C.H., S.S. and S.S.M. designed the experiments. C.H. performed all the experiments. C.H., S.S. analyzed the elemental composition. K.H., H.R.M., H.M.N. and D.S. supervised and assisted with the confocal microscopy experiments. P.K.W. supervised and assisted with NanoSIMS experiments and analysis. S.C. supervised and assisted with the XFM experiments. C.H., S.S. and S.S.M. prepared and edited the article.

Conflict of interest statement:

The authors have no conflict of interest to declare

Supplemental Figures Legends:

Supplemental Figure 1: S-content is not affected during growth

S content during logarithmic and stationary growth phase compared to cell density.

Supplemental Figure 2: Transcript changes in stationary cells do not show increased import capacities for trace metals

Transcript abundance analysis of transporters involved in Fe, Cu, Zn, P, Mn and Ca transport in late logarithmic, stationary, Fe-, Cu-, Zn- and P-limited conditions.

Supplemental Figure 3: Transient S accumulation in alkaline conditions correlates with biomass

S and C content comparison in alkaline conditions.

Supplemental Figure 4: Fe precipitates in cell-free TAP medium at pH 9.5 and higher

Analysis of the solubility of Fe in TAP growth medium at various alkaline pH points.

Supplemental Figure 5: Fe in alkaline conditions accumulates within cells in foci

Fe distribution, via the IP1 probe, chlorophyll and brightfield images of cells grown in pH 8.5 TAP medium with 20 or 200 µM Fe.

Supplemental Figure 6: LysoSensor identifies acidic compartments in alkaline cells

LysoSensor DND-189 detection of acidic pH compartments in cells grown in pH 7.0 or 8.5 TAP medium with 200 µM Fe.

Supplemental Figure 7: XFM shows Fe accumulate with Ca and P in alkaline conditions

S, P, Ca, Fe distribution and overlay in cells grown in pH 7 or pH 8.5 TAP medium with 200 µM Fe, as determined by X-ray fluorescence microscopy.

Supplemental Figure 8: NanoSIMS indicates Fe accumulate with Ca and P in alkaline conditions

Electron microscopy, C, Fe, P and Ca distribution (as determined via NanoSIMS) in cell sections of cultures grown in pH 7 and pH 8.5 TAP medium with 200 µM Fe.

Supplemental Figure 9: Subtle reduction of S, trace metal, Ca and P at elevated temperatures

Analysis of S, C, Fe, Cu, Zn, Mn, Ca, and P contents, normalized per cell, in cultures grown at 18, 21, 24, 27, and 30ºC.

Supplemental Figure 10: Vessel size does not affect growth or trace element quota

Analysis of growth and elemental composition of cells grown in different-sized vessels between 125- and 2800-ml capacity under replete or excess Fe condition (20 vs. 200 µM Fe).

Supplemental Figure 111: PCA

Pricipal component analyses of all individual experiments presented in the paper.

Supplemental Figure 122: Light quality spectrum

Light spectrum of the incubator used in all experiments, as measured in solution.

Supplemental Dataset 1: Transcript abundance estimates of transporters

Compiled expression estimates (FPKM) of the analyzed transporters in all analyzed datasets

References

Allen, M.D., del Campo, J.A., Kropat, J. and Merchant, S.S. (2007) *FEA1*, *FEA2*, and *FRE1*, encoding two homologous secreted proteins and a candidate ferrireductase, are expressed coordinately with *FOX1* and *FTR1* in iron-deficient *Chlamydomonas reinhardtii*. *Eukaryot Cell*, **6**, 1841-1852.

Andreini, C., Bertini, I., Cavallaro, G., Holliday, G.L. and Thornton, J.M. (2008) Metal ions in biological catalysis: from enzyme databases to general principles. *J Biol Inorg Chem*, **13**, 1205-1218.

Arcus, V.L., Prentice, E.J., Hobbs, J.K., Mulholland, A.J., Van der Kamp, M.W., Pudney, C.R., Parker, E.J. and Schipper, L.A. (2016) On the Temperature Dependence of Enzyme-Catalyzed Rates. *Biochemistry (Mosc).* **55**, 1681-1688.

Ariño, J., Ramos, J. and Sychrová, H. (2010) Alkali Metal Cation Transport and Homeostasis in Yeasts. *Microbiol. Mol. Biol. Rev.*, **74**, 95-120.

Au-Yeung, H.Y., Chan, J., Chantarojsiri, T. and Chang, C.J. (2013) Molecular Imaging of Labile Iron(II) Pools in Living Cells with a Turn-On Fluorescent Probe. *J. Am. Chem. Soc.*, **135**, 15165-15173.

Baxter, I.R., Vitek, O., Lahner, B., Muthukumar, B., Borghi, M., Morrissey, J., Guerinot, M.L. and Salt, D.E. (2008) The leaf ionome as a multivariable system to detect a plant's physiological status. *Proc. Natl. Acad. Sci. U. S. A.*, **105**, 12081-12086.

Behrenfeld, M.J., Westberry, T.K., Boss, E.S., O'Malley, R.T., Siegel, D.A., Wiggert, J.D., Franz, B.A., McClain, C.R., Feldman, G.C., Doney, S.C., Moore, J.K., Dall'Olmo, G., Milligan, A.J., Lima, I. and Mahowald, N. (2009) Satellite-detected fluorescence reveals global physiology of ocean phytoplankton. *Biogeosciences*, **6**, 779-794.

Beine-Golovchuk, O., Firmino, A.A.P., Dąbrowska, A., Schmidt, S., Erban, A., Walther, D., Zuther, E., Hincha, D.K. and Kopka, J. (2018) Plant Temperature Acclimation and Growth Rely on Cytosolic Ribosome Biogenesis Factor Homologs. *Plant Physiol.*, **176**, 2251-2276.

Berger, H., Blifernez-Klassen, O., Ballottari, M., Bassi, R., Wobbe, L. and Kruse, O. (2014) Integration of Carbon Assimilation Modes with Photosynthetic Light Capture in the Green Alga *Chlamydomonas reinhardtii*. *Mol Plant*, **7**, 1545-1559.

Blaby-Haas, C.E. and Merchant, S.S. (2012) The ins and outs of algal metal transport. *Biochim. Biophys. Acta*, **1823**, 1531-1552.

Blaby-Haas, C.E. and Merchant, S.S. (2013) Iron sparing and recycling in a compartmentalized cell. *Curr. Opin. Microbiol.*, **16**, 677-685.

Bonente, G., Pippa, S., Castellano, S., Bassi, R. and Ballottari, M. (2012) Acclimation of *Chlamydomonas reinhardtii* to Different Growth Irradiances. *J. Biol. Chem.*, **287**, 5833-5847.

Castro, C.D., Meehan, A.J., Koretsky, A.P. and Domach, M.M. (1995) In Situ ^{31}P Nuclear Magnetic Resonance for Observation of Polyphosphate and Catabolite Responses of Chemostat-Cultivated *Saccharomyces cerevisiae* after Alkalinization. *Appl. Environ. Microbiol.*, **61**, 4448-4453.

Castruita, M., Casero, D., Karpowicz, S.J., Kropat, J., Vieler, A., Hsieh, S.I., Yan, W., Cokus, S., Loo, J.A., Benning, C., Pellegrini, M. and Merchant, S.S. (2011) Systems Biology Approach in *Chlamydomonas* Reveals Connections between Copper Nutrition and Multiple Metabolic Steps. *Plant Cell*, **23**, 1273-1292.

Chen, S., Deng, J., Yuan, Y., Flachenecker, C., Mak, R., Hornberger, B., Jin, Q., Shu, D., Lai, B., Maser, J., Roehrig, C., Paunesku, T., Gleber, S.C., Vine, D.J., Finney, L., VonOsinski, J., Bolbat, M., Spink, I., Chen, Z., Steele, J., Trapp, D., Irwin, J., Feser, M., Snyder, E., Brister, K., Jacobsen, C., Woloschak, G. and Vogt, S. (2014) The Bionanoprobe: hard X-ray fluorescence nanoprobe with cryogenic capabilities. *J Synchrotron Radiat*, **21**, 66-75.

Crichton, R.R. (2008) 13 - Iron: Essential for Almost All Life. In *Biological Inorganic Chemistry* (Crichton, R.R. ed. Amsterdam: Elsevier, pp. 211-240.

Demmig-Adams, B., Dumlao, M.R., Herzenach, M.K. and Adams, W.W. (2008) Acclimation. In *Encyclopedia of Ecology* (Jørgensen, S.E. and Fath, B.D. eds). Oxford: Academic Press, pp. 15-23.

Docampo, R. (2006) Acidocalcisomes and Polyphosphate Granules. In *Inclusions in Prokaryotes* (Shively, J.M. ed. Berlin, Heidelberg: Springer Berlin Heidelberg, pp. 53-70.

Docampo, R., Scott, D.A., Vercesi, A.E. and Moreno, S.N. (1995) Intracellular Ca^{2+} storage in acidocalcisomes of *Trypanosoma cruzi*. *Biochem. J.*, **310 (Pt 3)**, 1005-1012.

Erickson, E., Wakao, S. and Niyogi, K.K. (2015) Light stress and photoprotection in *Chlamydomonas reinhardtii*. *Plant J.*, **82**, 449-465.

Gallaher, S.D., Fitz-Gibbon, S.T., Glaesener, A.G., Pellegrini, M. and Merchant, S.S. (2015) Chlamydomonas Genome Resource for Laboratory Strains Reveals a Mosaic of Sequence Variation, Identifies True Strain Histories, and Enables Strain-Specific Studies. *Plant Cell*, **27**, 2335-2352.

Gimpel, J.A., Specht, E.A., Georgianna, D.R. and Mayfield, S.P. (2013) Advances in microalgae engineering and synthetic biology applications for biofuel production. *Curr. Opin. Chem. Biol.*, **17**, 489-495.

Glaesener, A.G., Merchant, S.S. and Blaby-Haas, C.E. (2013) Iron economy in *Chlamydomonas reinhardtii*. *Front Plant Sci*, **4**, 337.

Goodenough, U., Heiss, A.A., Roth, R., Rusch, J. and Lee, J.H. (2019) Acidocalcisomes: Ultrastructure, Biogenesis, and Distribution in Microbial Eukaryotes. *Protist*, **170**, 287-313.

Gorman, D.S. and Levine, R.P. (1965) Cytochrome *f* and plastocyanin: Their sequence in the photosynthetic electron transport chain of *Chlamydomonas reinhardti**. *Proc. Natl. Acad. Sci. U. S. A.*, **54**, 1665-1669.

Grossman, A.R., Croft, M., Gladyshev, V.N., Merchant, S.S., Posewitz, M.C., Prochnik, S. and Spalding, M.H. (2007) Novel metabolism in Chlamydomonas through the lens of genomics. *Curr. Opin. Plant Biol.*, **10**, 190-198.

Harris, E.H. (2008) *The Chlamydomonas Sourcebook Second Edition Introduction to Chlamydomonas and Its Laboratory Use.* 2. edn. San Diego, CA: Elsevier/Academic Press.

Hemschemeier, A., Casero, D., Liu, B., Benning, C., Pellegrini, M., Happe, T. and Merchant, S.S. (2013) COPPER RESPONSE REGULATOR1–Dependent and –Independent Responses of the *Chlamydomonas reinhardtii* Transcriptome to Dark Anoxia. *Plant Cell*, **25**, 3186-3211.

Hong-Hermesdorf, A., Miethke, M., Gallaher, S.D., Kropat, J., Dodani, S.C., Chan, J., Barupala, D., Domaille, D.W., Shirasaki, D.I., Loo, J.A., Weber, P.K., Pett-Ridge, J., Stemmler, T.L., Chang, C.J. and Merchant, S.S. (2014) Subcellular metal imaging identifies dynamic sites of Cu accumulation in *Chlamydomonas*. *Nat Chem Biol*, **10**, 1034-1042.

Huang, Z., Shen, L., Wang, W., Mao, Z., Yi, X., Kuang, T., Shen, J.R., Zhang, X. and Han, G. (2021) Structure of photosystem I-LHCI-LHCII from the green alga *Chlamydomonas reinhardtii* in State 2. *Nat Commun*, **12**, 1100.

Hutner, S.H., Provasoli, L., Schatz, A. and Haskins, C.P. (1950) Some Approaches to the Study of the Role of Metals in the Metabolism of Microorganisms. *Proc. Am. Philos. Soc.*, **94**, 152-170.

Imlay, J.A. (2006) Iron-sulphur clusters and the problem with oxygen. *Mol. Microbiol.*, **59**, 1073-1082.

Imlay, J.A. (2008) Cellular defenses against superoxide and hydrogen peroxide. *Annu. Rev. Biochem.*, **77**, 755-776.

Imlay, J.A. (2014) The Mismetallation of Enzymes during Oxidative Stress. *J. Biol. Chem.*, **289**, 28121-28128.

James, G.O., Hocart, C.H., Hillier, W., Price, G.D. and Djordjevic, M.A. (2013) Temperature modulation of fatty acid profiles for biofuel production in nitrogen deprived Chlamydomonas reinhardtii. *Bioresour Technol*, **127**, 441-447.

Keasling, J.D. (1997) Regulation of Intracellular Toxic Metals and Other Cations by Hydrolysis of Polyphosphate. *Ann. N. Y. Acad. Sci.*, **829**, 242-249.

Kim, S.A., Punshon, T., Lanzirotti, A., Li, L., Alonso, J.M., Ecker, J.R., Kaplan, J. and Guerinot, M.L. (2006) Localization of Iron in *Arabidopsis* Seed Requires the Vacuolar Membrane Transporter VIT1. *Science*, **314**, 1295-1298.

Kropat, J., Gallaher, S.D., Urzica, E.I., Nakamoto, S.S., Strenkert, D., Tottey, S., Mason, A.Z. and Merchant, S.S. (2015) Copper economy in Chlamydomonas: prioritized allocation and reallocation of copper to respiration vs. photosynthesis. *Proc. Natl. Acad. Sci. U. S. A.*, **112**, 2644-2651.

Kropat, J., Hong-Hermesdorf, A., Casero, D., Ent, P., Castruita, M., Pellegrini, M., Merchant, S.S. and Malasarn, D. (2011) A revised mineral nutrient supplement increases biomass and growth rate in *Chlamydomonas reinhardtii*. *Plant J.*, **66**, 770-780.

Lavoie, M., Le Faucheur, S., Fortin, C. and Campbell, P.G. (2009) Cadmium detoxification strategies in two phytoplankton species: Metal binding by newly synthesized thiolated peptides and metal sequestration in granules. *Aquat Toxicol*, **92**, 65-75.

Li, X., Patena, W., Fauser, F., Jinkerson, R.E., Saroussi, S., Meyer, M.T., Ivanova, N., Robertson, J.M., Yue, R., Zhang, R., Vilarrasa-Blasi, J., Wittkopp, T.M., Ramundo, S., Blum, S.R., Goh, A., Laudon, M., Srikumar, T., Lefebvre, P.A., Grossman, A.R. and Jonikas, M.C. (2019) A genome-wide algal mutant library and functional screen identifies genes required for eukaryotic photosynthesis. *Nat. Genet.*, **51**, 627-635.

Li, X.P., Slavens, S., Crunkleton, D.W. and Johannes, T.W. (2021) Interactive effect of light quality and temperature on *Chlamydomonas reinhardtii* growth kinetics and lipid synthesis. *Algal Res*, **53**, 102127.

Lin, T.H., Rao, M.Y., Lu, H.W., Chiou, C.W., Lin, S.T., Chao, H.W., Zheng, Z.L., Cheng, H.C. and Lee, T.M. (2018) A role for glutathione reductase and glutathione in the tolerance of *Chlamydomonas reinhardtii* to photo-oxidative stress. *Physiol Plant*, **162**, 35-48.

Long, J.C. and Merchant, S.S. (2008) Photo-oxidative Stress Impacts the Expression of Genes Encoding Iron Metabolism Components in Chlamydomonas. *Photochem Photobiol.*, **84**, 1395-1403.

Lukeš, M., Procházková, L., Shmidt, V., Nedbalová, L. and Kaftan, D. (2014) Temperature dependence of photosynthesis and thylakoid lipid composition in the red snow alga *Chlamydomonas* cf. *nivalis* (*Chlorophyceae*). *FEMS Microbiol Ecol*, **89**, 303-315.

Lv, H., Qu, G., Qi, X., Lu, L., Tian, C. and Ma, Y. (2013) Transcriptome analysis of *Chlamydomonas reinhardtii* during the process of lipid accumulation. *Genomics*, **101**, 229-237.

Malasarn, D., Kropat, J., Hsieh, S.I., Finazzi, G., Casero, D., Loo, J.A., Pellegrini, M., Wollman, F.A. and Merchant, S.S. (2013) Zinc deficiency impacts CO_2 assimilation and disrupts copper homeostasis in *Chlamydomonas reinhardtii*. *J. Biol. Chem.*, **288**, 10672-10683.

Martínez-Muñoz, G.A. and Kane, P. (2008) Vacuolar and Plasma Membrane Proton Pumps Collaborate to Achieve Cytosolic pH Homeostasis in Yeast. *J. Biol. Chem.*, **283**, 20309-20319.

Massonnet, C., Vile, D., Fabre, J., Hannah, M.A., Caldana, C., Lisec, J., Beemster, G.T., Meyer, R.C., Messerli, G., Gronlund, J.T., Perkovic, J., Wigmore, E., May, S., Bevan, M.W., Meyer, C., Rubio-Díaz, S., Weigel, D., Micol, J.L., Buchanan-Wollaston, V., Fiorani, F., Walsh, S., Rinn, B., Gruissem, W., Hilson, P., Hennig, L., Willmitzer, L. and Granier, C. (2010) Probing the Reproducibility of Leaf Growth and Molecular Phenotypes: A Comparison of Three Arabidopsis Accessions Cultivated in Ten Laboratories. *Plant Physiol.*, **152**, 2142-2157.

Mengel, K. and Geurtzen, G. (1986) Iron chlorosis on calcareous soil. Alkaline nutritional condition as the cause for the chlorosis. *Journal of Plant Nutrition*, **9**, 161-173.

Merchant, S. and Bogorad, L. (1986) Regulation by copper of the expression of plastocyanin and cytochrome c552 in Chlamydomonas reinhardi. *Mol. Cell. Biol.*, **6**, 462-469.

Merchant, S.S. (2010) The Elements of Plant Micronutrients. *Plant Physiol.*, **154**, 512-515.

Merchant, S.S. and Helmann, J.D. (2012) Elemental Economy: Microbial Strategies for Optimizing Growth in the Face of Nutrient Limitation. *Adv. Microb. Physiol.*, **60**, 91-210.

Merchant, S.S., Prochnik, S.E., Vallon, O., Harris, E.H., Karpowicz, S.J., Witman, G.B., Terry, A., Salamov, A., Fritz-Laylin, L.K., Maréchal-Drouard, L., Marshall, W.F., Qu, L.H., Nelson, D.R., Sanderfoot, A.A., Spalding, M.H., Kapitonov, V.V., Ren, Q., Ferris, P., Lindquist, E., Shapiro, H., Lucas, S.M., Grimwood, J., Schmutz, J., Cardol, P., Cerutti, H., Chanfreau, G., Chen, C.L., Cognat, V., Croft, M.T., Dent, R., Dutcher, S., Fernández, E., Fukuzawa, H., González-Ballester, D., González-Halphen, D., Hallmann, A., Hanikenne, M., Hippler, M., Inwood, W., Jabbari, K., Kalanon, M., Kuras, R., Lefebvre, P.A., Lemaire, S.D., Lobanov, A.V., Lohr, M., Manuell, A., Meier,

I., Mets, L., Mittag, M., Mittelmeier, T., Moroney, J.V., Moseley, J., Napoli, C., Nedelcu, A.M., Niyogi, K., Novoselov, S.V., Paulsen, I.T., Pazour, G., Purton, S., Ral, J.P., Riaño-Pachón, D.M., Riekhof, W., Rymarquis, L., Schroda, M., Stern, D., Umen, J., Willows, R., Wilson, N., Zimmer, S.L., Allmer, J., Balk, J., Bisova, K., Chen, C.J., Elias, M., Gendler, K., Hauser, C., Lamb, M.R., Ledford, H., Long, J.C., Minagawa, J., Page, M.D., Pan, J., Pootakham, W., Roje, S., Rose, A., Stahlberg, E., Terauchi, A.M., Yang, P., Ball, S., Bowler, C., Dieckmann, C.L., Gladyshev, V.N., Green, P., Jorgensen, R., Mayfield, S., Mueller-Roeber, B., Rajamani, S., Sayre, R.T., Brokstein, P., Dubchak, I., Goodstein, D., Hornick, L., Huang, Y.W., Jhaveri, J., Luo, Y., Martínez, D., Ngau, W.C., Otillar, B., Poliakov, A., Porter, A., Szajkowski, L., Werner, G., Zhou, K., Grigoriev, I.V., Rokhsar, D.S. and Grossman, A.R. (2007) The *Chlamydomonas* Genome Reveals the Evolution of Key Animal and Plant Functions. *Science*, **318**, 245-250.

Merchant, S.S., Schmollinger, S., Strenkert, D., Moseley, J.L. and Blaby-Haas, C.E. (2020) From economy to luxury: Copper homeostasis in Chlamydomonas and other algae. *Biochimica et biophysica acta. Molecular cell research*, **1867**, 118822.

Mettler, T., Mühlhaus, T., Hemme, D., Schöttler, M.A., Rupprecht, J., Idoine, A., Veyel, D., Pal, S.K., Yaneva-Roder, L., Winck, F.V., Sommer, F., Vosloh, D., Seiwert, B., Erban, A., Burgos, A., Arvidsson, S., Schönfelder, S., Arnold, A., Günther, M., Krause, U., Lohse, M., Kopka, J., Nikoloski, Z., Mueller-Roeber, B., Willmitzer, L., Bock, R., Schroda, M. and Stitt, M. (2014) Systems Analysis of the Response of Photosynthesis, Metabolism, and Growth to an Increase in Irradiance in the Photosynthetic Model Organism *Chlamydomonas reinhardtii*. *Plant Cell*, **26**, 2310-2350.

Morales-Sánchez, D., Schulze, P.S.C., Kiron, V. and Wijffels, R.H. (2020) Temperature-Dependent Lipid Accumulation in the Polar Marine Microalga *Chlamydomonas malina* RCC2488. *Front Plant Sci*, **11**, 619064.

Morel, F.M.M., Hudson, R.J.M. and Price, N.M. (1991) Limitation of productivity by trace metals in the sea. *Limnology and Oceanography*, **36**, 1742-1755.

Moroney, J.V., Ma, Y., Frey, W.D., Fusilier, K.A., Pham, T.T., Simms, T.A., DiMario, R.J., Yang, J. and Mukherjee, B. (2011) The carbonic anhydrase isoforms of *Chlamydomonas reinhardtii*: intracellular location, expression, and physiological roles. *Photosynth Res*, **109**, 133-149.

Moseley, J., Quinn, J., Eriksson, M. and Merchant, S. (2000) The *Crd1* gene encodes a putative di-iron enzyme required for photosystem I accumulation in copper deficiency and hypoxia in *Chlamydomonas reinhardtii*. *EMBO J.*, **19**, 2139-2151.

Moseley, J.L., Allinger, T., Herzog, S., Hoerth, P., Wehinger, E., Merchant, S. and Hippler, M. (2002) Adaptation to Fe-deficiency requires remodeling of the photosynthetic apparatus. *EMBO J.*, **21**, 6709-6720.

Moseley, J.L., Chang, C.W. and Grossman, A.R. (2006) Genome-based approaches to understanding phosphorus deprivation responses and PSR1 control in Chlamydomonas reinhardtii. *Eukaryot Cell*, **5**, 26-44.

Padilla-López, S. and Pearce, D.A. (2006) *Saccharomyces cerevisiae* Lacking Btn1p Modulate Vacuolar ATPase Activity to Regulate pH Imbalance in the Vacuole. *J. Biol. Chem.*, **281**, 10273-10280.

Park, J., McCormick, S.P., Chakrabarti, M. and Lindahl, P.A. (2013) The Lack of Synchronization between Iron Uptake and Cell Growth Leads to Iron Overload in *Saccharomyces cerevisiae* during Post-exponential Growth Modes. *Biochemistry (Mosc).* **52**, 9413-9425.

Pazour, G.J. and Witman, G.B. (2009) Chapter 15 - The *Chlamydomonas* Flagellum as a Model for Human Ciliary Disease. In *The Chlamydomonas Sourcebook (Second Edition)* (Harris, E.H., Stern, D.B. and Witman, G.B. eds). London: Academic Press, pp. 445-478.

Pivato, M. and Ballottari, M. (2021) *Chlamydomonas reinhardtii* cellular compartments and their contribution to intracellular calcium signalling. *Journal of experimental botany*, **72**, 5312-5335.

Porter, A.S., Evans-Fitz Gerald, C., McElwain, J.C., Yiotis, C. and Elliott-Kingston, C. (2015) How well do you know your growth chambers? Testing for chamber effect using plant traits. *Plant methods*, **11**, 44.

Rodriguez, I.B. and Ho, T.Y. (2017) Interactive effects of spectral quality and trace metal availability on the growth of *Trichodesmium* and *Symbiodinium*. *PLOS ONE*, **12**, e0188777.

Römheld, V., Müller, C. and Marschner, H. (1984) Localization and Capacity of Proton Pumps in Roots of Intact Sunflower Plants. *Plant Physiol.*, **76**, 603-606.

Sager, R. and Granick, S. (1953) Nutritional studies with *Chlamydomonas reinhardi*. *Ann. N. Y. Acad. Sci.*, **56**, 831-838.

Salt, D.E., Baxter, I. and Lahner, B. (2008) Ionomics and the Study of the Plant Ionome. *Annu Rev Plant Biol*, **59**, 709-733.

Santi, S. and Schmidt, W. (2009) Dissecting iron deficiency-induced proton extrusion in Arabidopsis roots. *The New phytologist*, **183**, 1072-1084.

Schmollinger, S., Chen, S., Strenkert, D., Hui, C., Ralle, M. and Merchant, S.S. (2021) Single-cell visualization and quantification of trace metals in *Chlamydomonas* lysosome-related organelles. *Proc. Natl. Acad. Sci. U. S. A.*, **118**, e2026811118.

Schmollinger, S., Muhlhaus, T., Boyle, N.R., Blaby, I.K., Casero, D., Mettler, T., Moseley, J.L., Kropat, J., Sommer, F., Strenkert, D., Hemme, D., Pellegrini, M., Grossman, A.R., Stitt, M., Schroda, M. and Merchant, S.S. (2014) Nitrogen-Sparing Mechanisms in *Chlamydomonas* Affect the Transcriptome, the Proteome, and Photosynthetic Metabolism. *Plant Cell*, **26**, 1410-1435.

Scott, D.A., Docampo, R., Dvorak, J.A., Shi, S. and Leapman, R.D. (1997) *In Situ* Compositional Analysis of Acidocalcisomes in *Trypanosoma cruzi*. *J. Biol. Chem.*, **272**, 28020-28029.

Serra-Cardona, A., Canadell, D. and Ariño, J. (2015) Coordinate responses to alkaline pH stress in budding yeast. *Microb Cell*, **2**, 182-196.

Serrano, R., Bernal, D., Simón, E. and Ariño, J. (2004) Copper and Iron Are the Limiting Factors for Growth of the Yeast *Saccharomyces cerevisiae* in an Alkaline Environment. *J. Biol. Chem.*, **279**, 19698-19704.

Sharma, S.S., Dietz, K.J. and Mimura, T. (2016) Vacuolar compartmentalization as indispensable component of heavy metal detoxification in plants. *Plant Cell Environ*, **39**, 1112-1126.

Shen, L., Huang, Z., Chang, S., Wang, W., Wang, J., Kuang, T., Han, G., Shen, J.R. and Zhang, X. (2019) Structure of a $C_2S_2M_2N_2$-type PSII-LHCII supercomplex from the green alga *Chlamydomonas reinhardtii*. *Proc. Natl. Acad. Sci. U. S. A.*, **116**, 21246-21255.

Silflow, C.D. and Lefebvre, P.A. (2001) Assembly and Motility of Eukaryotic Cilia and Flagella. Lessons from *Chlamydomonas reinhardtii Plant Physiol.*, **127**, 1500-1507.

Stephenson, P.G., Moore, C.M., Terry, M.J., Zubkov, M.V. and Bibby, T.S. (2011) Improving photosynthesis for algal biofuels: toward a green revolution. *Trends Biotechnol.*, **29**, 615-623.

Strenkert, D., Limso, C.A., Fatihi, A., Schmollinger, S., Basset, G.J. and Merchant, S.S. (2016) Genetically Programmed Changes in Photosynthetic Cofactor Metabolism in Copper-deficient Chlamydomonas. *J. Biol. Chem.*, **291**, 19118-19131.

Sunda, W. and Huntsman, S. (2003) Effect of pH, light, and temperature on Fe–EDTA chelation and Fe hydrolysis in seawater. *Marine Chemistry*, **84**, 35-47.

Sunda, W.G. and Huntsman, S.A. (1995) Iron uptake and growth limitation in oceanic and coastal phytoplankton. *Marine Chemistry*, **50**, 189-206.

Theil, E.C. (1987) Ferritin: Structure, gene, regulation, and celluar function in animals, plants and microorganisms. *Annu. Rev. Biochem.*, **56**, 289-315.

Tsednee, M., Castruita, M., Salomé, P.A., Sharma, A., Lewis, B.E., Schmollinger, S.R., Strenkert, D., Holbrook, K., Otegui, M.S., Khatua, K., Das, S., Datta, A., Chen, S., Ramon, C., Ralle, M., Weber, P.K., Stemmler, T.L., Pett-Ridge, J., Hoffman, B.M. and Merchant, S.S. (2019) Manganese co-localizes with calcium and phosphorus in *Chlamydomonas* acidocalcisomes and is mobilized in manganese-deficient conditions. *J. Biol. Chem.*, **294**, 17626-17641.

Urzica, E.I., Casero, D., Yamasaki, H., Hsieh, S.I., Adler, L.N., Karpowicz, S.J., Blaby-Haas, C.E., Clarke, S.G., Loo, J.A., Pellegrini, M. and Merchant, S.S. (2012) Systems and trans-system level analysis identifies conserved iron deficiency responses in the plant lineage. *Plant Cell*, **24**, 3921-3948.

Vogt, S. (2013) MAPS: A set of software tools for analysis and visualization of 3D X-ray fluorescence data sets. *J. Phys. IV*, **104**, 635–638.

Waldron, K.J., Rutherford, J.C., Ford, D. and Robinson, N.J. (2009) Metalloproteins and metal sensing. *Nature*, **460**, 823-830.

Wang, L., Xiao, L., Yang, H., Chen, G., Zeng, H., Zhao, H. and Zhu, Y. (2020) Genome-Wide Identification, Expression Profiling, and Evolution of Phosphate Transporter Gene Family in Green Algae. *Frontiers in Genetics*, **11**.

Wang, W.Y. (1978) Effect of Dim Light on the *y-1* Mutant of *Chlamydomonas reinhardtii*. *Plant Physiol.*, **61**, 842-846.

Figure legends

Figure 1: P, Ca, Fe, Cu, and Zn accumulate in stationary Chlamydomonas

(A) Percentage of photon flux density (PFD, in µmol photons·m^{-2}·s^{-1}) in growing cultures at different cell densities vs. cell-free growth medium. (B) Growth curve, doubling time (C) and number of generations between inoculation and stationary phase (D) of wild-type Chlamydomonas cultures (CC-4533) grown in 20 µM (black) or 200 µM (red) Fe-containing TAP media. Fe (E), Cu (F), Zn (G), Mn (H), Ca (I), and P (J) content, normalized to total cellular S content, during growth were measured using ICP-MS/MS. Averages are shown with error bars indicating standard deviation of three independent cultures. R^2 values correspond to linear regression fitting of the time points in stationary phase. Asterisks indicate significant differences (t-test, $p \leq 0.05$) between the 20 and 200 µM Fe conditions.

Figure 2: Ca and Zn content increase at higher light intensities

Doubling time (A) and number of generations from inoculation until stationary phase (B) of cultures grown in 20 or 200 µM Fe at the indicated PFDs in culture. Cell-associated Fe (C), Cu (D), Zn (E), Mn (F), Ca (G), and P (H) abundance, as measured by ICP-MS/MS, collected during mid-log growth (2-4 x 10^6 cells/ml) at the indicated PFDs in culture. Averages are shown with error bars indicating standard deviation of three independent cultures. *a* and *b* indicate significance (t-test, $p \leq 0.017$, multiple Bonferroni-corrected) to cells grown at 95 µmol m^{-2} s^{-1} in 20 (*a*) or 200 µM Fe (*b*).

Figure 3: Exclusively Fe accumulates at high pH

(A) pH of the spent media during growth of Chlamydomonas cultures in TAP media containing 20 (black) or 200 (red) µM Fe, inoculated at 10^4 cells/ml either at pH 7.0 (filled circles, slid line) or pH 8.5 (open circles, dotted line). Lines represent the best exponential fittings for the pH values. The doubling time of the cultures is shown in (B), the total number of generations from inoculation until stationary phase is shown in (C). Fe (D), Cu (E), Zn (F), Mn (G), Ca (H), and P (I) content, normalized to total cellular S content, of the cells during growth were measured using ICP-MS/MS. The cells were collected during mid-log growth (2-4 x 10^6 cells/ml), the corresponding Fe concentration and pH of the

growth media are as indicated. Asterisks indicate significant differences (t-test, $p \leq 0.05$) to cells grown in 20 µM Fe at pH 7. Averages are shown with error bars indicating standard deviation of three independent cultures.

Figure 4: Alkaline accumulated Fe co-localizes with P and Ca

(A) Fe and chlorophyll distribution in cells grown in TAP medium with 20 or 200 µM Fe at pH 8.5. IP1 was used to determine the Fe(II) distribution (violet). Depicted is the Fe(II) distribution and an overlay of Fe(II) (violet) with chlorophyll autofluorescence (Chl, green) and the brightfield image (BF) in three cells; additional cells can be found in Supplemental Figure 5. The confocal images were collected on a Zeiss LSM 880 microscope. Scale bar = 2 µm. (B) From left to right, P, Ca, Fe distribution and overlay (P = blue; Ca = red; Fe = green) in three cells grown in pH 8.5 or pH 7 TAP medium with 200 µM Fe, determined by X-ray fluorescence microscopy. The elemental distributions are depicted between the minimal (black) and maximal (white) elemental concentrations in µg/cm^2, which are denoted in the bottom right and top right corner of each image. Scale bar = 2 µm. Cell outlines and S distribution in these cells can be found in Supplemental Figure 7. (C) From left to right, P, Ca and Fe distribution of a cell section from a culture grown in pH 8.5 TAP medium with 200 µM Fe, determined with NanoSIMS. Sections of fixed cells were imaged in positive secondary ion mode, scale bar = 5 µm. Additional cells at lower resolution can be found in Supplemental Figure 8. (D) Correlative quantification of C-normalized Fe, P and Ca content from NanoSIMS images of cells grown in pH 8.5 (top, filled circles) or pH 7 (bottom, open circles) TAP medium with 200 µM Fe. Each data point corresponds to a non-overlapping region in the images. R^2 values are derived from a linear regression fitting of all data points in each plot.

Figure 5: Zn content is elevated at decreased temperatures

Doubling time (A) and number of generations (B) between inoculation and stationary phase of cells grown at the indicated temperatures under replete (20 µM) or excess (200 µM) Fe conditions. Cell-associated Fe (C), Cu (D), Zn (E), Mn (F), Ca (G) and P (H) content at the indicated temperatures under replete (20 µM) and excess (200 µM) Fe conditions, as measured by ICP-MS/MS during mid-log growth (2-4 x 10^6 cells/ml).

Averages are shown with error bars indicating standard deviation of 3 independent cultures. *a* and *b* indicate significant differences (t-test, $p \leq 0.013$, multiple Bonferroni-corrected) to cells grown at 24ºC with 20 µM Fe (*a*) or 200 µM Fe (*b*).

Figure 6: Cu accumulates at low shaking speeds

Doubling time (A) and number of generations between inoculation and stationary phase (B) of cells grown with shaking speed between 0 and 180 RPM under replete or excess Fe condition (20 vs. 200 µM Fe). Cell-associated Fe (C), Cu (D), Zn (E), Mn (F), Ca (G) and P (H) content under replete (20 µM) and excess (200 µM) Fe conditions, as measured by ICP-MS/MS during mid-log growth (2-4 x 10^6 cells/ml). *a* and *b* indicate significant differences (t-test, $p \leq 0.013$, multiple Bonferroni-corrected) to cells grown at 180 rpm with 20 µM Fe (*a*) or 200 µM Fe (*b*). Averages are shown with error bars indicating standard deviation of three independent cultures.

Figure 7: Fill-fraction of growth vessel affects growth rate and Mn content

Doubling time (A) and number of generations between inoculation and stationary (B) of cells grown in between 10 and 80% filled flasks under replete or excess Fe condition (20 vs. 200 µM Fe). Cell-associated Fe (C), Cu (D), Zn (E), Mn (F), Ca (G) and P (H) content under replete (20 µM) and excess (200 µM) Fe conditions, as measured by ICP-MS/MS during mid-log growth (2-4 x 10^6 cells/ml). Averages are shown with error bars indicating standard deviation of three independent cultures. *a* and *b* indicate significant differences (t-test, $p \leq 0.013$, multiple Bonferroni-corrected) to cells grown at 40% fill-level with 20 µM Fe (*a*) or 200 µM Fe (*b*).

Figure 8: Growth and elemental profile of common laboratory wild-type strains of Chlamydomonas

Doubling time (A) and number of generations between inoculation and stationary (B) of cells from the indicated Chlamydomonas strains grown in replete (20 µM) and excess (200 µM) Fe conditions. Cell-associated Fe (C), Cu (D), Zn (E), Mn (F), Ca (G) and P (H) content under replete (20 µM) and excess (200 µM) Fe conditions, as measured by ICP-MS/MS during mid-log growth (2-4 x 10^6 cells/ml). Averages are shown with error bars indicating standard deviation of three independent cultures. *a* and *b* indicate significant

differences (t-test, $p \leq 0.013$, multiple Bonferroni-corrected) to CC-4533 with 20 µM Fe (*a*) or 200 µM Fe (*b*).

Figure 9: Comparison of elemental signatures between all different environmental perturbations

Principal component analysis (PCA) separating alga samples according to their elemental composition in the various growth experiments. Each point corresponds to an elemental composition in a single environmental condition (average of three replicates each). Points are filled grey for cultures grown in 20 µM Fe, or filled red when grown in 200 µM Fe. Outlines indicate the experiment the samples originated from, either from the cell density (black), light intensity (yellow), pH (pink), flask size (cyan), culture volume (green), shaking speed (orange), temperature (log phase – brown, stationary phase – violet) or strain (dark green) experiment. The percentage of the total variance accounted for by the first and second principal component are indicated on the axes.

Figures

Figure 1: P, Ca, Fe, Cu, and Zn accumulate in stationary Chlamydomonas

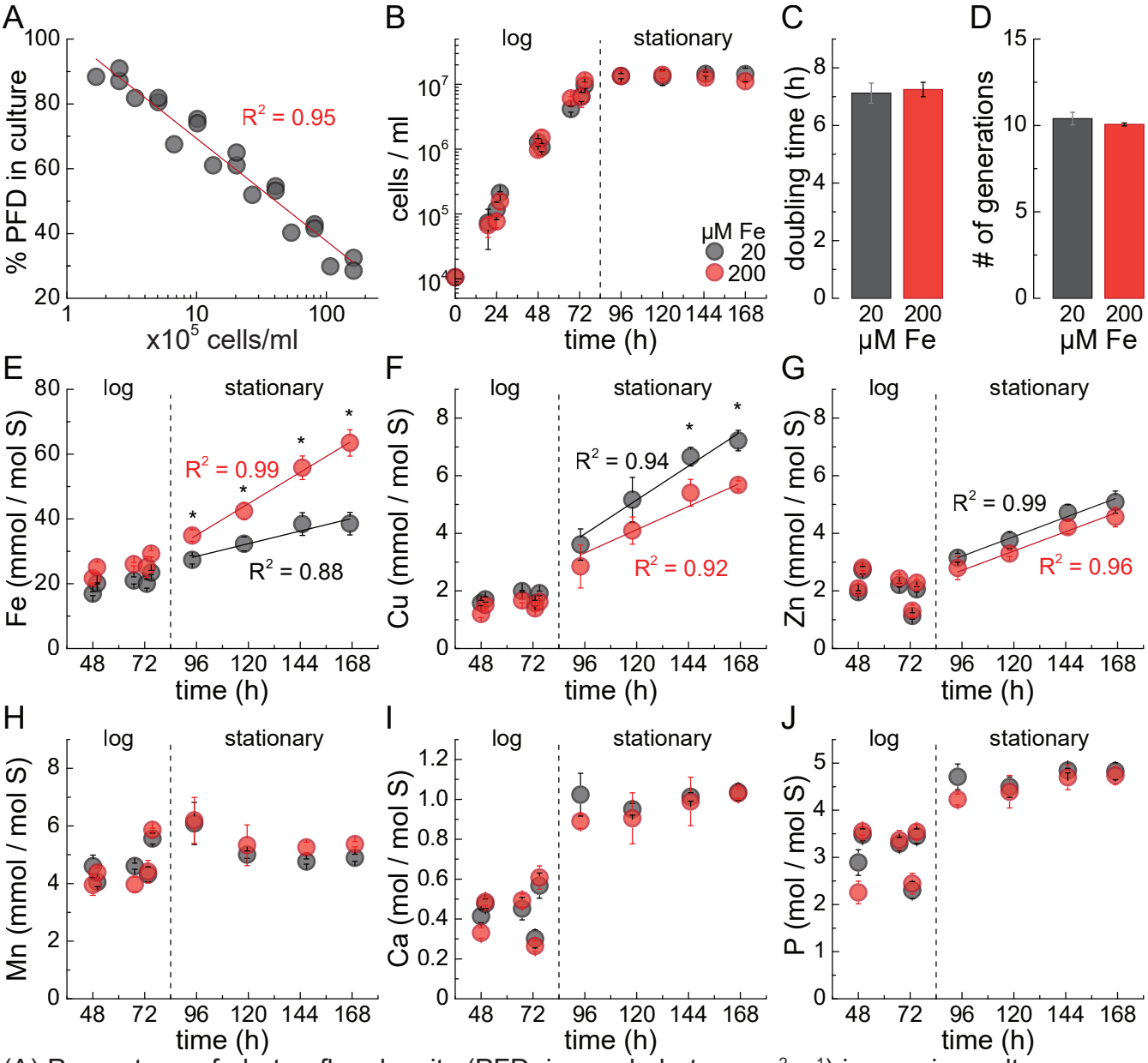

(A) Percentage of photon flux density (PFD, in μmol photons·m^{-2}·s^{-1}) in growing cultures at different cell densities vs. cell-free growth medium. (B) Growth curve, doubling time (C) and number of generations between inoculation and stationary phase (D) of wild-type Chlamydomonas cultures (CC-4533) grown in 20 μM (black) or 200 μM (red) Fe-containing TAP media. Fe (E), Cu (F), Zn (G), Mn (H), Ca (I), and P (J) content, normalized to total cellular S content, during growth were measured using ICP-MS/MS. Averages are shown with error bars indicating standard deviation of three independent cultures. R^2 values correspond to linear regression fitting of the time points in stationary phase. Asterisks indicate significant differences (t-test, $p < 0.05$) between the 20 and 200 μM Fe conditions.

Figure 2: Ca and Zn content increase at higher light intensities

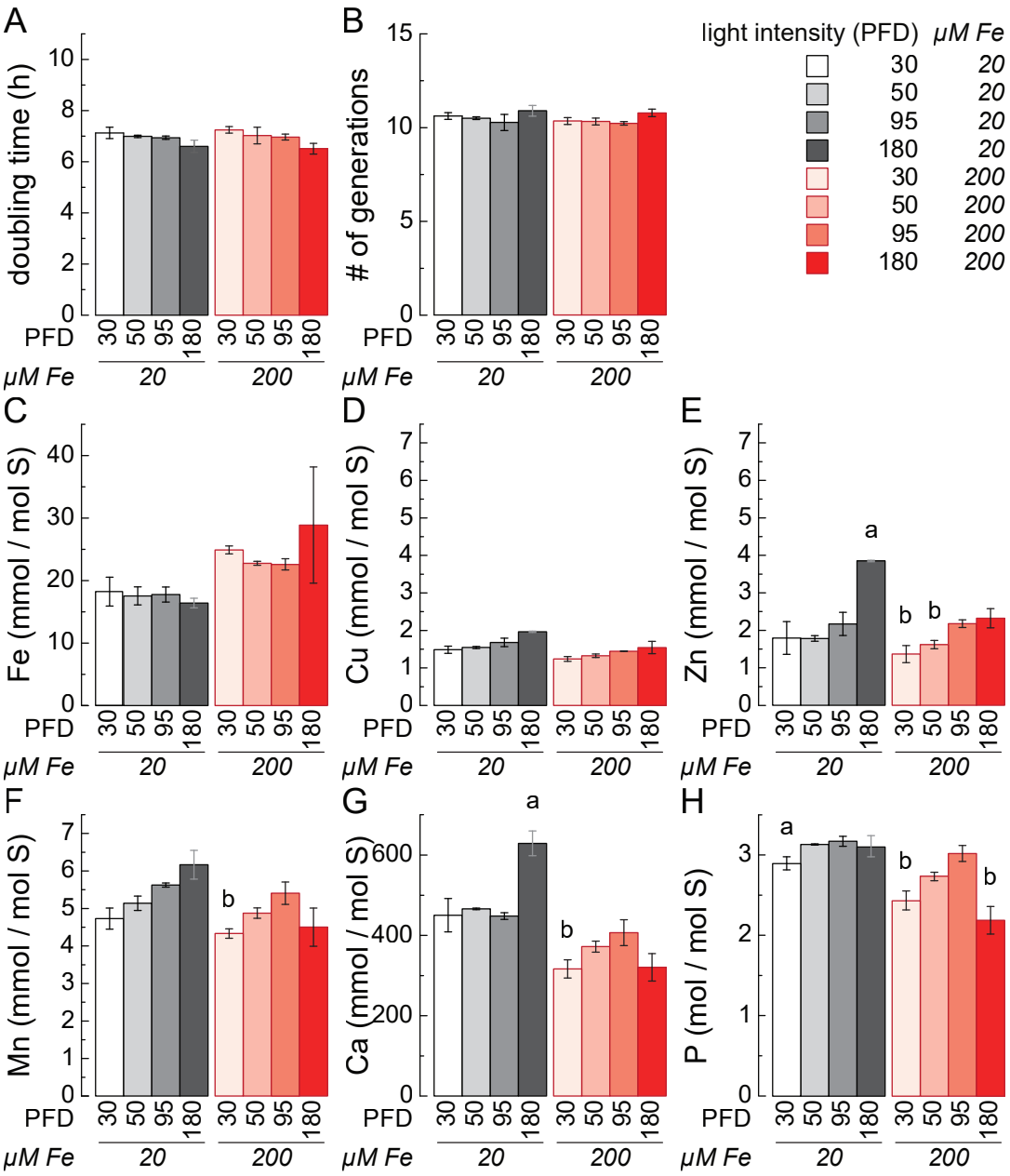

Doubling time (A) and number of generations from inoculation until stationary phase (B) of cultures grown in 20 or 200 µM Fe at the indicated PFDs in culture. Cell-associated Fe (C), Cu (D), Zn (E), Mn (F), Ca (G), and P (H) abundance, as measured by ICP-MS/MS, collected during mid-log growth (2-4 x 10^6 cells/ml) at the indicated PFDs in culture. Averages are shown with error bars indicating standard deviation of three independent cultures. a and b indicate significance (t-test, $p < 0.017$, multiple Bonferroni-corrected) to cells grown at 95 µmol m^{-2} s^{-1} in 20 (a) or 200 µM Fe (b).

Figure 3: Exclusively Fe accumulates at high pH

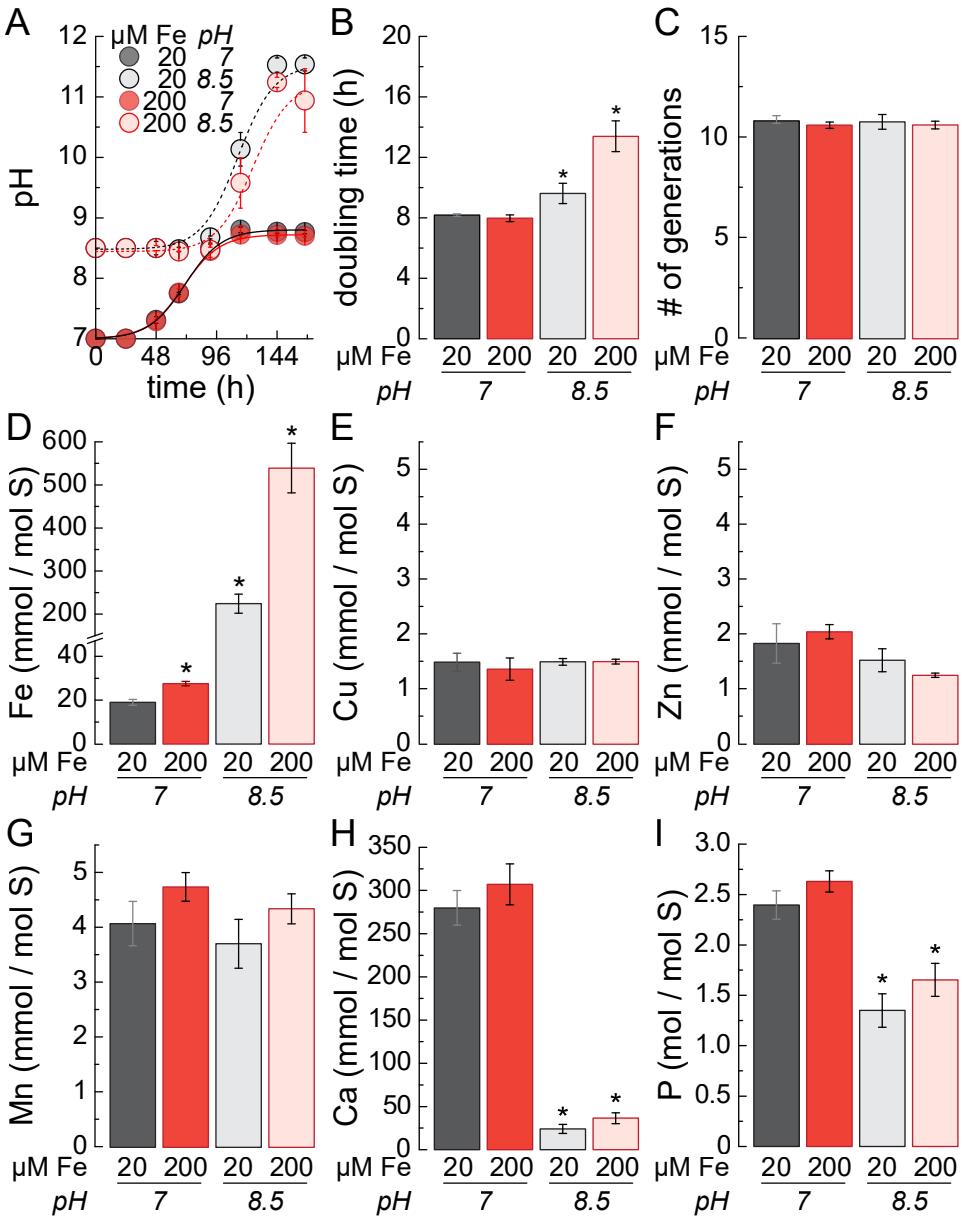

(A) pH of the spent media during growth of Chlamydomonas cultures in TAP media containing 20 (black) or 200 (red) μM Fe, inoculated at 10^4 cells/ml either at pH 7 (filled circles, slid line) or pH 8.5 (open circles, dotted line). Lines represent the best exponential fittings for the pH values. The doubling time of the cultures is shown in (B), the total number of generations from inoculation until stationary phase is shown in (C). Fe (D), Cu (E), Zn (F), Mn (G), Ca (H), and P (I) content, normalized to total cellular S content, of the cells during growth were measured using ICP-MS/MS. The cells were collected during mid-log growth (2-4 x 10^6 cells/ml), the corresponding Fe concentration and pH of the growth media are as indicated. Asterisks indicate significant differences (t-test, $p < 0.05$) to cells grown in 20 μM Fe at pH 7. Averages are shown with error bars indicating standard deviation of three independent cultures.

Figure 4: Alkaline accumulated Fe co-localizes with P and Ca

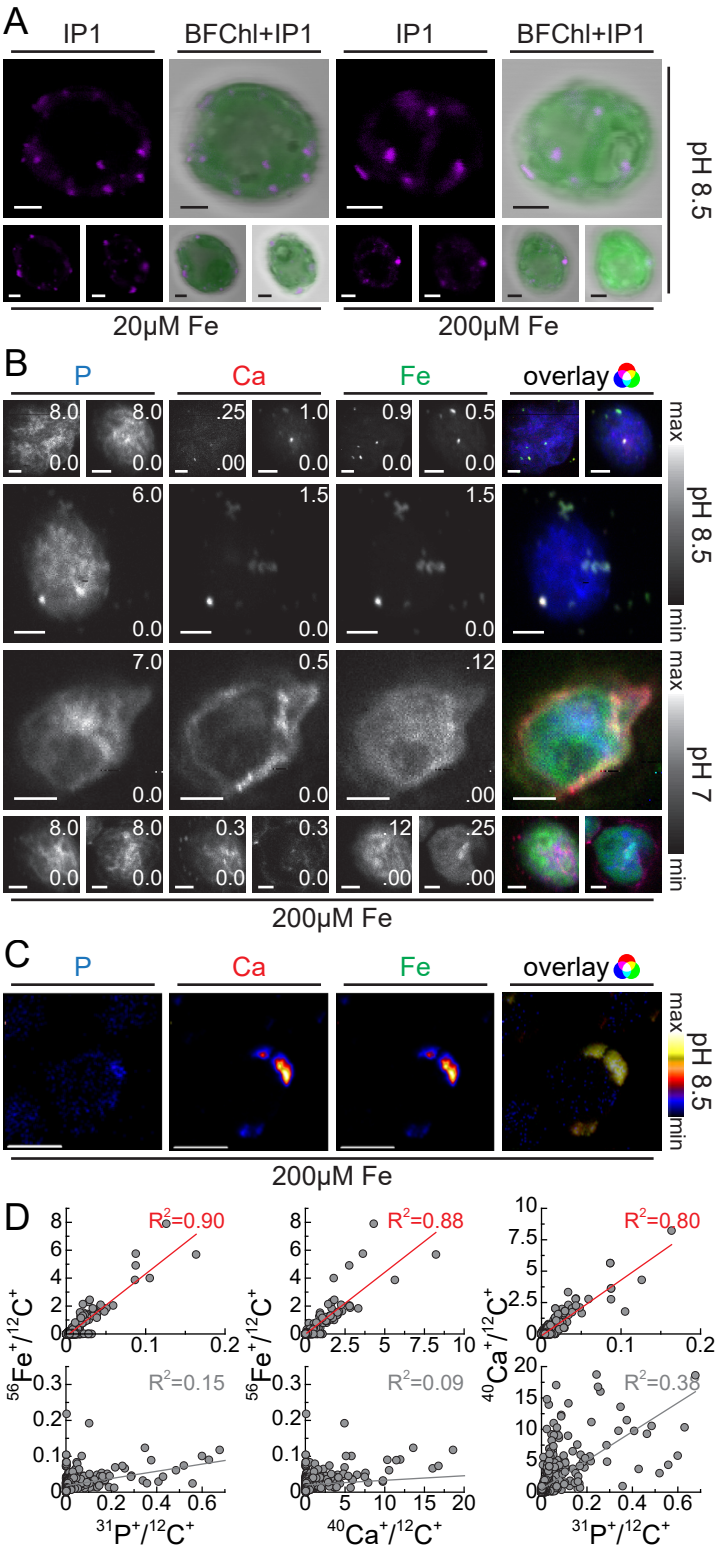

(A) Fe and chlorophyll distribution in cells grown in TAP medium with 20 or 200 µM Fe at pH 8.5. IP1 was used to determine the Fe(II) distribution (violet). Depicted is the Fe(II) distribution and an overlay of Fe(II) (violet) with chlorophyll autofluorescence (Chl, green) and the brightfield image (BF) in three cells; additional cells can be found in Supplemental Figure 5. The confocal images were collected on a Zeiss LSM 880 microscope. Scale bar = 2 µm. (B) From left to right, P, Ca, Fe distribution and overlay (P = blue; Ca = red; Fe = green) in three cells grown in pH 8.5 or pH 7 TAP medium with 200 µM Fe, determined by X-ray fluorescence microscopy. The elemental distributions are depicted between the minimal (black) and maximal (white) elemental concentrations in µg/cm^2, which are denoted in the bottom right and top right corner of each image. Scale bar = 2 µm. Cell outlines and S distribution in these cells can be found in 6. (C) From left to right, P, Ca and Fe distribution of a cell section from a culture grown in pH 8.5 TAP medium with 200 µM Fe, determined with NanoSIMS. Sections of fixed cells were imaged in positive secondary ion mode, scale bar = 5 µm. Additional cells at lower resolution can be found in 7. (D) Correlative quantification of C-normalized Fe, P and Ca content from NanoSIMS images of cells grown in pH 8.5 (top, filled circles) or pH 7 (bottom, open circles) TAP medium with 200 µM Fe. Each data point corresponds to a non-overlapping region in the images. R^2 values are derived from a linear regression fitting of all data points in each plot.

Figure 5: Zn content is elevated at decreased temperatures

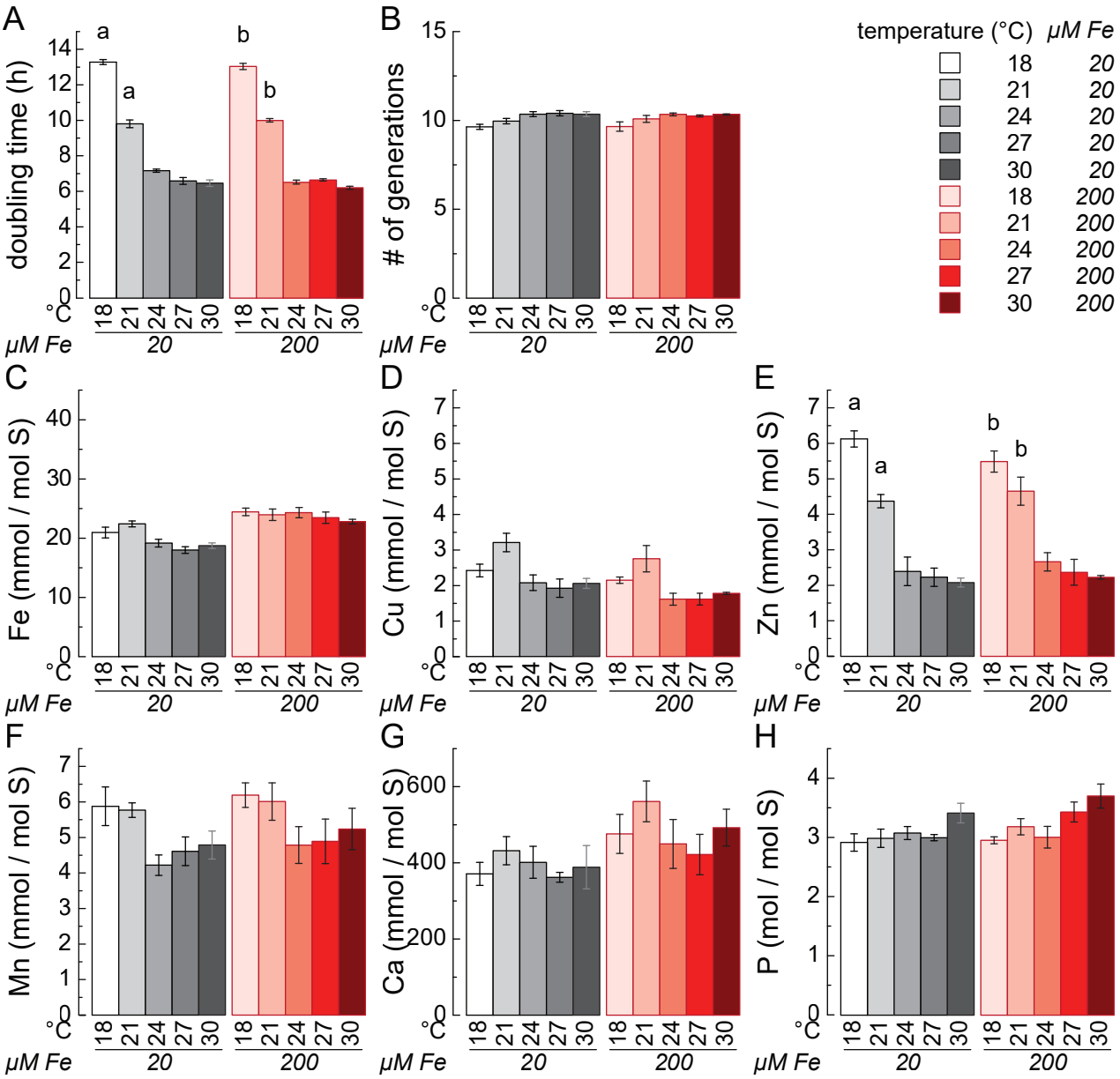

Doubling time (A) and number of generations (B) between inoculation and stationary phase of cells grown at the indicated temperatures under replete (20 µM) or excess (200 µM) Fe conditions. Cell-associated Fe (C), Cu (D), Zn (E), Mn (F), Ca (G) and P (H) content at the indicated temperatures under replete (20 µM) and excess (200 µM) Fe conditions, as measured by ICP-MS/MS during mid-log growth (2-4 x 10^6 cells/ml). Averages are shown with error bars indicating standard deviation of 3 independent cultures. a and b indicate significant differences (t-test, $p < 0.013$, multiple Bonferroni-corrected) to cells grown at 24ºC with 20 µM Fe (a) or 200 µM Fe (b).

Figure 6: Cu accumulates at low shaking speeds

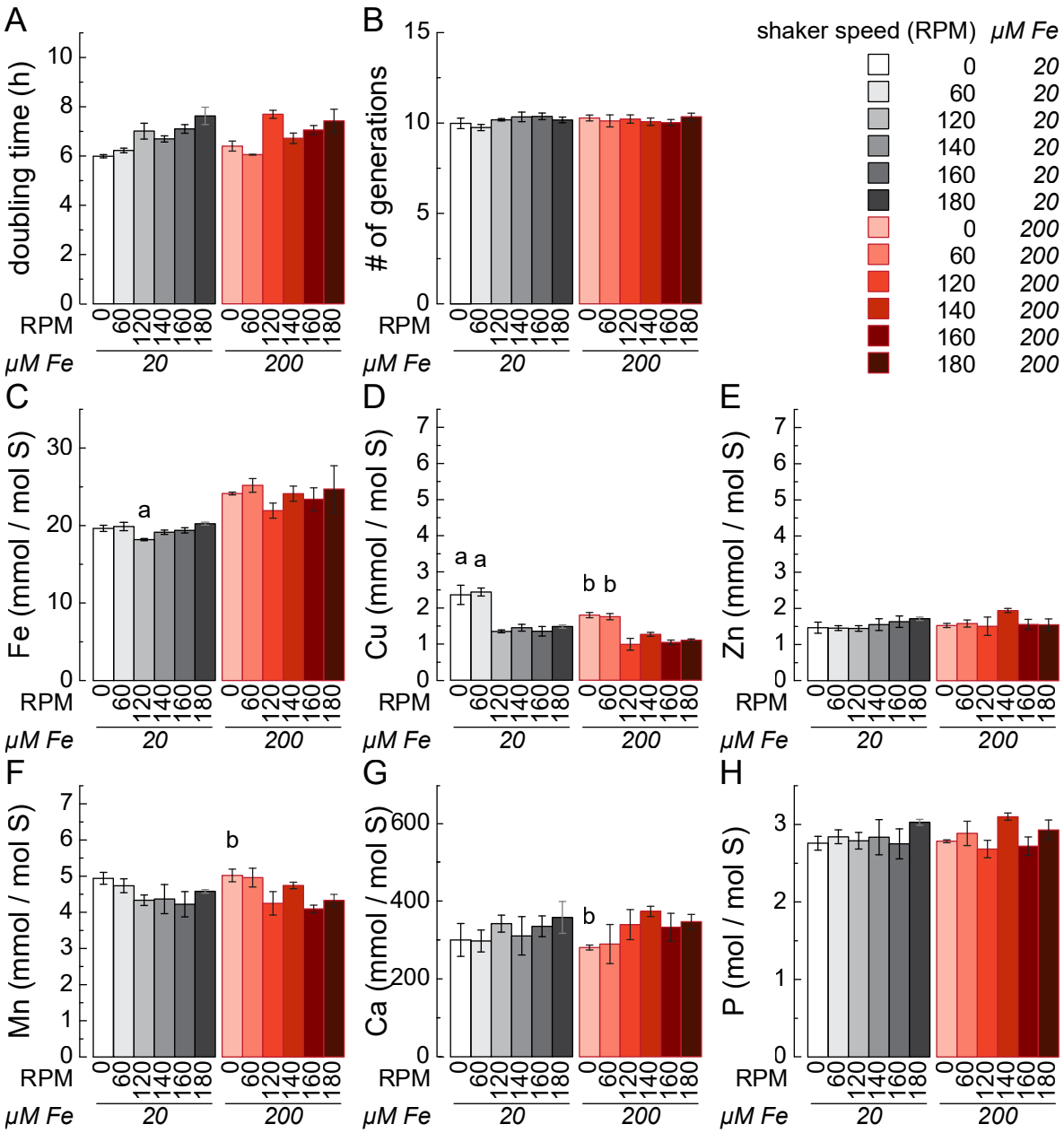

Doubling time (A) and number of generations between inoculation and stationary phase (B) of cells grown with shaking speed between 0 and 180 RPM under replete or excess Fe condition (20 vs. 200 µM Fe). Cell-associated Fe (C), Cu (D), Zn (E), Mn (F), Ca (G) and P (H) content under replete (20 µM) and excess (200 µM) Fe conditions, as measured by ICP-MS/MS during mid-log growth (2-4 x 10^6 cells/ml). a and b indicate significant differences (t-test, $p < 0.013$, multiple Bonferroni-corrected) to cells grown at 180 rpm with 20 µM Fe (a) or 200 µM Fe (b). Averages are shown with error bars indicating standard deviation of three independent cultures.

Figure 7: Fill-fraction of growth vessel affects growth rate and Mn content

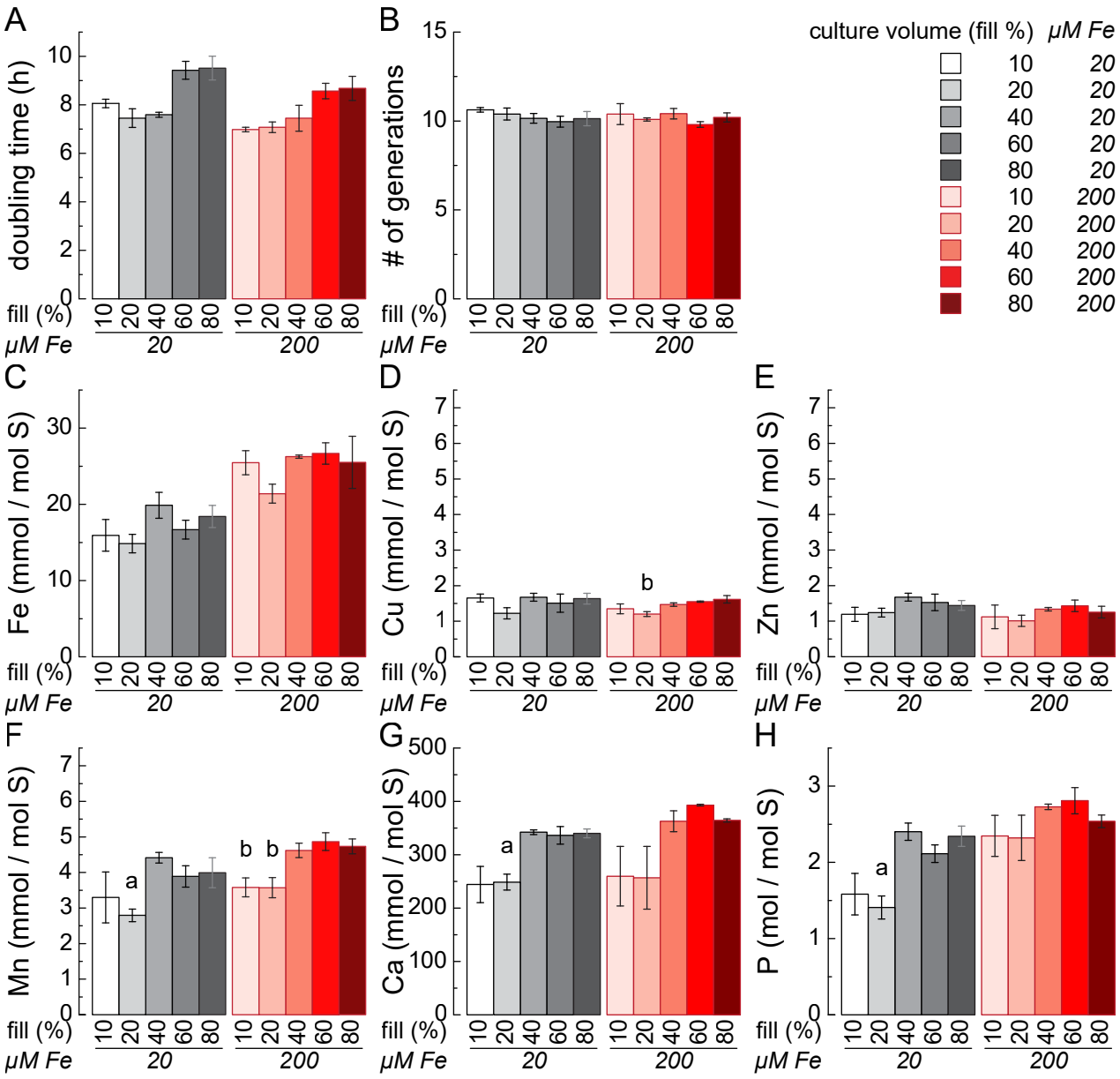

Doubling time (A) and number of generations between inoculation and stationary (B) of cells grown in between 10 and 80% filled flasks under replete or excess Fe condition (20 vs. 200 µM Fe). Cell-associated Fe (C), Cu (D), Zn (E), Mn (F), Ca (G) and P (H) content under replete (20 µM) and excess (200 µM) Fe conditions, as measured by ICP-MS/MS during mid-log growth (2-4 x 10^6 cells/ml). Averages are shown with error bars indicating standard deviation of three independent cultures. a and b indicate significant differences (t-test, $p < 0.013$, multiple Bonferroni-corrected) to cells grown at 40% fill-level with 20 µM Fe (a) or 200 µM Fe (b).

Figure 8: Growth and elemental profile of common laboratory wild-type strains of Chlamydomonas

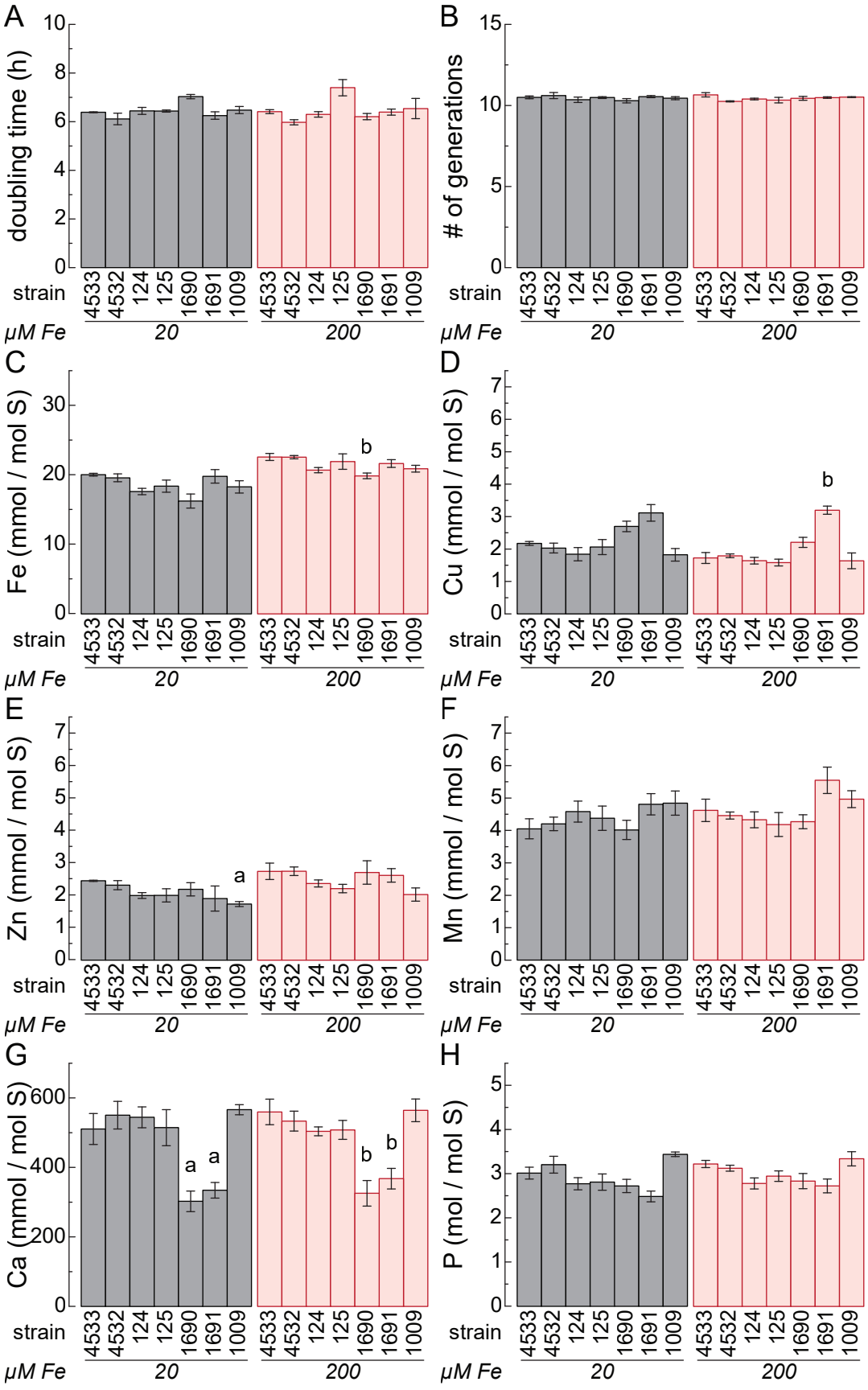

Doubling time (A) and number of generations between inoculation and stationary (B) of cells from the indicated Chlamydomonas strains grown in replete (20 µM) and excess (200 µM) Fe conditions. Cell-associated Fe (C), Cu (D), Zn (E), Mn (F), Ca (G) and P (H) content under replete (20 µM) and excess (200 µM) Fe conditions, as measured by ICP-MS/MS during mid-log growth (2-4 x 10^6 cells/ml). Averages are shown with error bars indicating standard deviation of three independent cultures. a and b indicate significant differences (t-test, $p < 0.013$, multiple Bonferroni-corrected) to CC-4533 with 20 µM Fe (a) or 200 µM Fe (b).

Figure 9: Comparison of elemental signatures between all different environmental perturbations

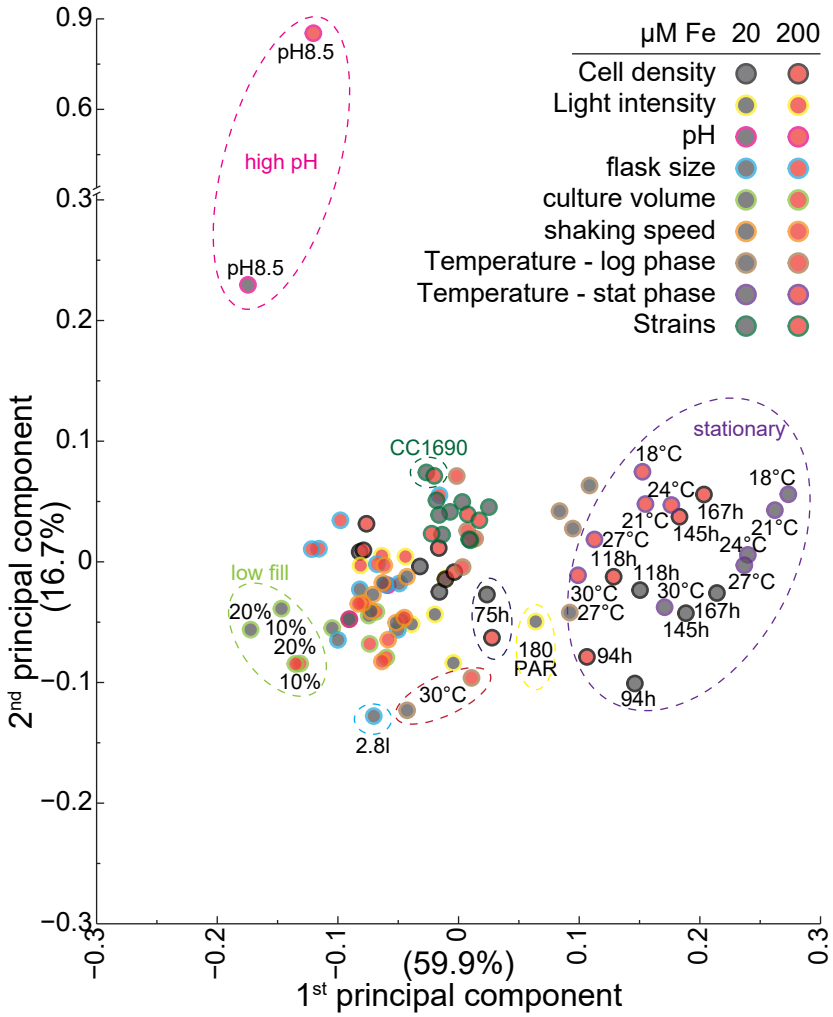

Principal component analysis (PCA) separating alga samples according to their elemental composition in the various growth experiments. Each point corresponds to an elemental composition in a single environmental condition (average of three replicates each). Points are filled grey for cultures grown in 20 μM Fe, or filled red when grown in 200 μM Fe. Outlines indicate the experiment the samples originated from, either from the cell density (black), light intensity (yellow), pH (pink), flask size (cyan), culture volume (green), shaking speed (orange), temperature (log phase – brown, stationary phase – violet) or strain (dark green) experiment. The percentage of the total variance accounted for by the first and second principal component are indicated on the axes.